POLARIZATION MAINTAINING AND SPECTRAL FILTERING PROPERTIES OF HOLLOW-CORE OPTICAL FIBERS FOR NEAR-INFRARED REGION

A THESIS SUBMITTED TO

THE GRADUATE SCHOOL OF ENGINEERING AND SCIENCE

OF BILKENT UNIVERSITY

IN PARTIAL FULFILLMENT OF THE REQUIREMENTS FOR

THE DEGREE OF

MASTER OF SCIENCE

IN

MATERIALS SCIENCE AND NANOTECHNOLOGY

By

Muhammad Zain Siddiqui

August 2024

POLARIZATION MAINTAINING AND SPECTRAL FILTERING PROPERTIES OF HOLLOW-CORE OPTICAL FIBERS FOR NEAR-INFRARED REGION
By Muhammad Zain Siddiqui
August 2024

We certify that we have read this thesis and that in our opinion it is fully adequate, in scope and in quality, as a thesis for the degree of Master of Science.

Mustafa Ordu(Advisor)

Bülend Ortaç

Ahmet E. Akosman

Approved for the Graduate School of Engineering and Science:

Orhan Arıkan
Director of the Graduate School

ABSTRACT

POLARIZATION MAINTAINING AND SPECTRAL FILTERING PROPERTIES OF HOLLOW-CORE OPTICAL FIBERS FOR NEAR-INFRARED REGION

Muhammad Zain Siddiqui
M.S. in Materials Science and Nanotechnology
Advisor: Mustafa Ordu
August 2024

Negative curvature hollow-core fibers (NCFs) offer attractive properties like ultra-low losses, broad bandwidth, low latency, low nonlinearity, and a high damage threshold. Additionally, NCFs can overcome the inherent optical transparency limitations posed by solid-core fibers, which restrict their application to specific wavebands, thus enabling more flexible usage of NCF. These qualities make NCFs suitable for their utilization as polarization-maintaining (PM) fibers. In this thesis, the PM properties of NCFs are investigated through two different design approaches. In the first part of the thesis, a new design of polarization-maintaining and spectral filtering NCF tailored for the telecommunication bands in the near-infrared region is presented. The optical fiber, consisting of a six-tube silica structure, incorporates nested tubes anchored radially by pole structures in the vertical direction. Meanwhile, in the horizontal direction, nested tubes without pole anchors are employed, making the fiber structure asymmetric, which encounters birefringence. This unique fiber design not only preserves the polarization states of light but also exhibits frequency selective transmission exclusively in the vertical direction due to the pole structure. Through numerical modeling, transmission losses below 0.1 dB/km for spectrally filtered wavelengths are achieved, with birefringence on the order of 10^{-5} within the spectral range of 1.45 μm to 1.60 μm. These results demonstrate significant improvements in terms of birefringence, distinct loss separation between horizontally and vertically polarized states, and a reduced number of spectrally filtered wavelengths compared to previously reported findings. The proposed fiber design holds untapped potential for applications requiring selective transmission with specific polarization. The second part of the thesis focuses on the effect of ellipticity on the polarization-maintaining performance of NCFs. The nested tube NCF is stretched vertically and compressed horizontally with the same ellipticity of 5%, 8%, and 10% to introduce ellipticity through the entire cross-section of the fiber. Through these modifications, the fiber successfully exhibits orthogonal polarization states compared to the original fiber with no ellipticity. Further investigations into the fiber with 8% ellipticity involve coupling it with bi-thickness (t_1 and t_2) and a manipulated nested tube diameter (d_{nx}) along the horizontal axis of the fiber. The findings reveal that ellipticity has a limited effect on the improvement of the birefringence and polarization extinction ratio (PER) in NCFs, but it can be used as a complementary fine-tuning process. This suggests that ellipticity has the potential to be utilized as an additional mechanism for enhancing the overall polarization-maintaining characteristics of NCFs.

Keywords: Hollow-core negative curvature fibers (NCFs), Polarization maintaining fibers, PM fibers, Spectral filtering, Selective transmission.

ÖZET

YAKIN KIZILÖTESİ BÖLGESİ İÇİN DELİK ÇEKİRDEKLİ OPTİK FİBERLERİN POLARİZASYON KORUNUM VE SPEKTRAL FİLTRELEME ÖZELLİKLERİ

Muhammad Zain Siddiqui
Malzeme Bilimi ve Nanoteknoloji, Yüksek Lisans
Tez Danışmanı: Mustafa Ordu
Ağustos 2024

Delik çekirdekli negatif eğrilikli fiberler (NCF), düşük kayıplı ışık iletimi, geniş bant açıklığı, düşük gecikme süresi, düşük doğrusal olmayan optik etkiler ve yüksek hasar eşiği gibi ilgi çekici özellikler sunmaktadır. Ayrıca, NCF'ler, katı çekirdekli fiberlerin belirli dalga boylarındaki doğal optik iletim sınırlamalarının üstesinden gelebilir ve böylece NCF'lere daha esnek bir kullanım imkanı tanır. Bu özellikler, NCF'leri polarizasyon-korumalı (PM) fiberler olarak kullanımı için uygun hale getirmektedir. Bu tezde, NCF'lerin PM özellikleri, iki farklı tasarım yaklaşımı üzerinden incelenmektedir. Tezin ilk bölümünde, telekomünikasyon bantlarına yönelik polarizasyon korumalı ve spektral filtreleme özelliklerine sahip yeni bir NCF tasarımı sunulmaktadır. Altı borulu silika yapıdan oluşan optik fiber, dikey yönde çubuk yapılarıyla radyal olarak sabitlenmiş iç içe geçmiş borular içermektedir. Bu esnada, yatay yönde çubuk bağlantısı olmayan iç içe geçmiş borular kullanılmaktadır. Bu, fiber yapısını asimetrikleştirir ve çift kırınım oluşturur. Ortaya çıkan özgün fiber tasarımı, ışığın polarizasyon durumlarını korumakla kalmaz, aynı zamanda dikey çubuklu yapısı sayesinde yalnızca dikey yönde frekans seçici bir iletim gösterir. Sayısal modelleme yoluyla, spektral olarak filtrelenmiş dalga boyları için 0.1 dB/km'nin altında iletim kayıpları elde edilmiş, çift kırınım ise $1.45\,\mu m$ ile $1.60\,\mu m$ spektral aralığında 10^{-5} mertebesinde gerçekleşmiştir. Bu sonuçlar, çift kırınım, yatay ve dikey polarize konumları arasında belirgin kayıp ayrımı ve önceki bulgulara kıyasla spektral olarak filtrelenmiş dalgaboylarının sayısında azalma açısından önemli iyileştirmeler göstermektedir. Önerilen fiber tasarımı, belirli polarizasyonlar ile seçici iletimler gerektiren uygulamalar için keşfedilmemiş potansiyele sahiptir. Tezin ikinci bölümü, eliptikliğin NCF'lerde polarizasyon koruma performansı üzerindeki etkisine odaklanmaktadır. İç içe geçmiş borulu NCF, fiberin tüm kesiti boyunca eliptiklik oluşturmak için dikeyde esnetilmiş ve yatayda sıkıştırılmıştır. Bu değişikliklerle fiber, eliptikliği olmayan orijinal fiberle karşılaştırıldığında başarılı bir şekilde ortogonal polarizasyon durumları sergilemiştir. Fiberde %8'lik eliptiklikle yapılan incelemeler sonucunda, fiberin yatay ekseni boyunca çift kalınlık (t_1 ve t_2) ve manipüle edilmiş iç içe geçmiş boru çapı (d_{nx}) ile eşleştirilmesini içermektedir. Sonuçlar, eliptikliğin NCF'lerde çift kırılma ve polarizasyon sönümlenme oranına (PER) kısıtlı fayda sağladığı, bunu yanında genel polarizasyon koruma özelliklerini artırmak için tamamlayıcı bir ince ayar süreci olarak kullanılabileceğini ortaya koymaktadır. Bu, eliptikliğin NCF'lerde ek bir mekanizma olarak kullanılma potansiyeline sahip olduğunu göstermektedir.

Anahtar sözcükler: Delik-Çekirdekli Negatif Eğrilikli Fiberler, Polarizasyon-Korumalı Fiberler, Spektral Filtreleme, Seçici İletim.

Acknowledgement

Firstly, I sincerely appreciate my supervisor, Dr. Mustafa Ordu, for his unwavering support, supervision, motivation, and mentorship throughout my master's journey. When I was searching for positions with a limited research background, he accepted me in his research group, Contemporary Fibers Laboratory (CFL), for which I am deeply grateful to him. He provided me with a platform where I was given the freedom to not only learn and grow myself but also to share and implement my ideas. Besides being an academic supervisor, he also acted as a counselor in my non-academic life. Furthermore, I am grateful to Asst. Prof. Bülend Ortaç and Asst. Prof. Ahmet E. Akosman, my thesis committee members, for their valuable insights and comments.

I acknowledge UNAM, Bilkent University, and TÜBİTAK for providing an excellent environment, facilities, and financial aid to undertake my research work. I am also thankful to all the Faculty, Engineers, and Administrative Staff of UNAM for helping and guiding me whenever I was in need. I am genuinely thankful to the past and present members of the CFL group: Asfandyar Khan, Md Kawsar Ahmed, Md Mehdi Hasan, Mahmudur Rahman, Arda Kurucu, Md Sazid Bin Sadeque, Syed Zubair Hussain, Deniz Berk Onuralp, Arooj Fatima, Samet Akçimen, Cihat Kürşat Kalkan, and Göktan Yılmaz for a wonderful experience working together and for the genuine assistance whenever needed.

I built some valuable friendships while pursuing my Master's studies at Bilkent University, which did not make me feel away from home. I want to especially thank Najeeb, Badar, Waqar, Usama, Rashid, Hilal Bhai, Talha, Muzaffar, Ahsan, Mansoor, Osama Adil, Mohsin, Shakir, Faiqa, Dr Iqra, Robab, Amir, Rayan, Salahuddin Bhai, Imran Bhai, and Usman Bhai for their support and amazing time we had together. Salman Zafar, my friend from my bachelor's degree class, deserves special mention because his constant encouragement made it possible for me to start my Master's studies at Bilkent University.

I would like to mention my lovely wife, Musham, whom I married in 2022 during my Master's studies. She has been a constant supporter and motivator throughout my journey. Above all, none of this would have been possible without the love, support, hard work, and sacrifices of my dear parents, Muhammad Shamim Siddiqui(late) and Imrana Shamim. I will never be able to express in words how much I appreciate everything they have done for me. I am especially thankful to my siblings for all the support they gave me to pursue my MS in Türkiye while they took care of our dear mother in Pakistan.

Contents

List of Figures

Chapter 1

Introduction

1.1 Hollow-core optical fibers (HCFs)

Optical fibers have excelled as waveguides for long-distance light transmission. Conventional solid-core optical fibers are broadly used in various applications, including telecommunications, high-power beam delivery, fiber lasers, and sensing [1, 2, 3, 4, 5]. They have a higher refractive index material core at the center and a lower refractive index material cladding surrounding the core for effective light guiding through total internal reflection. The guided modes in these fibers have an effective refractive index in between the refractive indices of cladding and core [6]. Hollow-core fibers (HCFs) have gathered great interest among the fiber optics community due to their remarkable properties like ultra-low loss, high data transfer rate, low non-linearity, and high optical damage threshold [7, 8, 9, 10]. In HCFs, air (sometimes other gases or liquids) is used mostly in the hollow-core region with a refractive index lower than the surrounding cladding material. Therefore, the light-guidance mechanism in HCFs differs from that of solid-core fibers. Fig. 1.1 shows a schematic illustration of the difference between the guidance mechanisms of solid and hollow-core fibers. Different theories have been proposed in the literature for light guidance in HCFs. Based on those light guidance mechanisms, HCFs are divided into two types: hollow-core photonic bandgap fibers (HC-PBGFs), which relies on the photonic bandgap effect to guide the light, while hollow-core antiresonant fibers (HC-ARFs) relies on a combination of antiresonant reflection optical waveguide (ARROW) model, and the inhibited coupling (IC) mechanism.

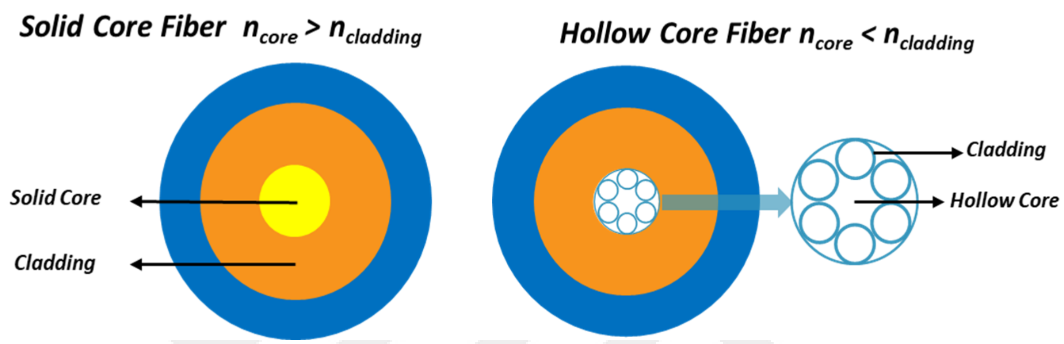

Figure 1.1: Comparison of solid-core fibers with hollow-core fibers (HCFs).

1.1.1 Hollow-core photonic bandgap fibers (HC-PBGFs)

A hollow-core photonic bandgap fiber (HC-PBGF) confines the light through the photonic bandgap effect, which is formed by periodic variations of high and low refractive index materials [11]. A bandgap signifies that certain frequencies of light cannot propagate through HC-PBGF. Only when the frequency of light falls within the bandgap range can the periodic cladding structure confine the light within the central hollow core. HC-PBGFs offer low-loss light transmission with low non-linearity, low latency, and a higher damage threshold than solid-core fibers [11, 12]. The first single-mode HC-PBGF was demonstrated in 1999 after it gathered much attention in the 1990s due to its exceptional properties that overcame the limitations of traditional step-index fibers [13]. Despite the narrow bandwidth offered by HC-PBGFs, they possess reduced transmission losses compared to conventional solid-core fibers. Further reduction in transmission losses for HC-PBGF is constrained due to the presence of surface modes at the nodes formed by the micro-structured cladding membranes [14]. A scanning electron microscope (SEM) micrograph of the HC-PBGF cross section is shown in Fig. 1.2(a).

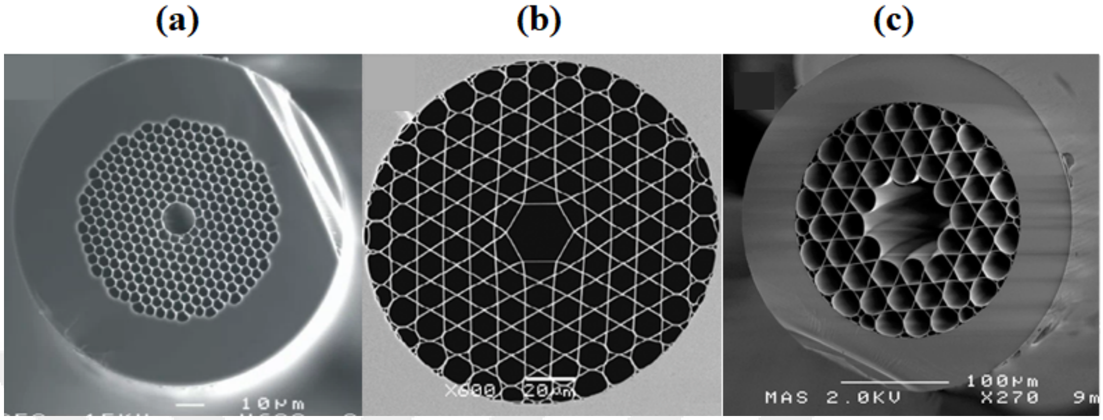

Figure 1.2: SEM images of various HCFs (a) HC-PBGF [15], HC-ARFs (b) and (c) Kagome fibers with straight core surround and hypocycloid core surround [16].

1.1.2 Hollow-core antiresonant fibers (HC-ARFs)

A hollow-core antiresonant fiber (HC-ARF) is known for its low loss and broadband guidance [17, 18]. HC-ARF depends on the antiresonant reflection optical waveguide (ARROW) model and inhibited coupling (IC) mechanism for light guidance. The ARROW model states that the high refractive index layer surrounding the hollow-core region serves as a Fabry-Pérot resonator [19], and the transverse field is reflected back at the core in antiresonance frequencies. In other words, the dielectric layers produce constructive back reflections to the hollow-core region within a specific frequency range, functioning like a mirror, and the reflectivity is determined by the refractive index and thickness of the dielectric layers. Meanwhile, the inhibited coupling (IC) mechanism refers to the strong confinement of the fundamental core mode within the core region, achieved by significantly preventing coupling between the core and cladding modes. This reduction in coupling is accomplished by creating a large effective index mismatch and minimizing the field overlap integral between the core and cladding modes [10]. Kagome fiber was among the first HC-ARFs demonstrating broadband low-loss transmission [20]. Although Kagome fibers exhibit higher transmission loss than HC-PBGFs, they provide a broad bandwidth with tunable dispersion [21, 22]. An SEM image of a cross-section of a Kagome fiber is illustrated in Fig. 1.2(b).

1.1.2.1 Negative curvature hollow-core fibers (NCFs)

More research on Kagome fibers led to the finding that a hollow core surrounded by negative curvature in HCFs can achieve more efficient light confinement. This leads to ultra-low loss transmission with broad bandwidth. Fig. 1.2(c) depicts an SEM image of a Kagome fiber with a negative curvature core surround. This revelation started the development of a new promising type of HC-ARFs known as negative curvature hollow-core fibers (NCFs) [10, 23, 24, 25, 26, 27, 28]. It is worth mentioning that in the literature, NCFs are sometimes referred to as inhibited coupling HCFs (IC-HCFs), hollow-core photonic crystal fibers (HCPCFs), or hollow-core antiresonant fibers (HC-ARFs). In this thesis, NCFs will be used to refer to these fibers for simplicity.

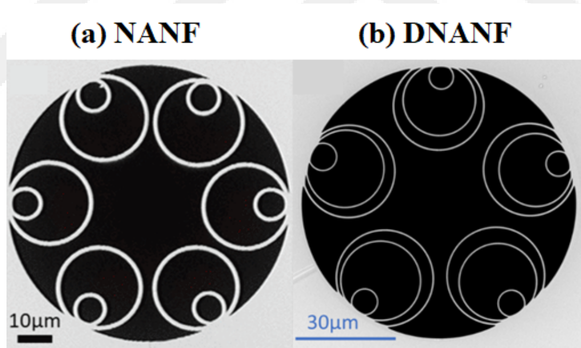

Figure 1.3: SEM images of (a) nested antiresonant nodeless fiber (NANF) [29] and (b) double nested antiresonant nodeless fiber (DNANF) [30].

NCFs offered broadband reduced transmission losses, many other desirable optical properties, and simplified fabrication compared to HC-PBGFs. Therefore, NCFs became the ideal candidate for future fiber optics development. The breakthrough NCF design of nested antiresonant nodeless fiber (NANF) in 2014 by F. Poletti [25] showed promising capabilities of NCF to lower the propagation losses below the fundamental limit of solid core fibers, which is 0.15 dB/km. In 2018, the first NANF was fabricated, which showed the lowest loss of 1.3 dB/km at 1.45 μm achieved by any HCF [29]. Further optimization of NANF design leads to double nested antiresonant nodeless fiber (DNANF), which was fabricated in 2022 and showed the lowest loss of 0.174 dB/km across the C-band [30]. Just recently, DNANF was fabricated with extensive optimization of geometry, which showed the lowest propagation loss < 0.11 dB/km at 1.55 μm ever achieved in an optical fiber [31]. SEM images of NANF and DNANF are shown in Fig. 1.3(a) and Fig. 1.3(b), respectively.

These remarkable advancements in NCFs highlight their potential for further development in specialized optical fibers, particularly for applications requiring precise propagation control for the polarization state of light. Such specialized optical fibers are called polarization-maintaining (PM) optical fibers. In the following sections, we will delve deeper into the details of PM fibers.

1.2 Polarization maintaining (PM) optical fibers

In single-mode fibers, the fundamental core mode is a degenerate combination of two orthogonal polarization modes [32]. These orthogonal polarization states can be regarded as horizontal and vertical polarizations along the x and y axes of the fiber, respectively, as shown in Fig. 1.4. In conventional telecommunication type fibers (non-PM), these two states possess the same propagation constant (transmit at the same velocities through fiber). Consequently, optical energy can easily cross-couple from one polarization state to another if these fibers undergo any perturbation or disturbance. In an ideal non-PM fiber having perfect radial symmetry, the input polarization state remains unchanged as it propagates along the fiber. However, non-PM fibers experience unavoidable disruptions, like bending, environmental temperature variations, pressure effects, etc., which break the fiber's rotational symmetry, causing different propagation constants for the orthogonal polarization states. Therefore, the fiber exhibits polarization mode dispersion (PMD), or we can say birefringence is induced into the fiber [32].

Fiber optic gyroscopes [33], fiber sensors [34], spectroscopy [35], and PM optical amplifiers [36] are applications that require the polarization state of light to be preserved to provide a consistent output signal for better sensing accuracy. Since conventional non-PM fibers cannot be protected from external perturbations and cannot retain their polarization state, PM fibers are purposely designed

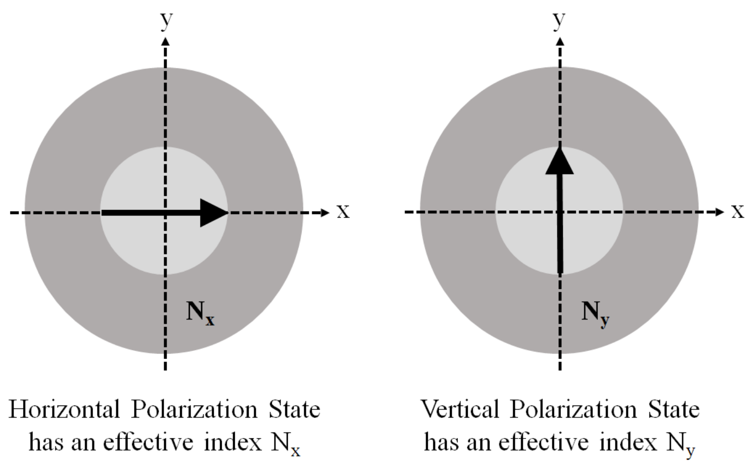

Figure 1.4: Horizontal and vertical polarization states in a single mode fiber.

with an anisotropic core. Consequently, two orthogonal polarization states must propagate with different propagation constants. Therefore, PM fibers have built-in high birefringence, ensuring that the input polarization state is maintained throughout the fiber.

Traditional solid core PM fibers introduce high birefringence in the core through stress and form anisotropy. Stress elements are equipped in stress birefringent fibers to achieve high birefringence, like in PANDA and Bowtie fibers [37, 38]. While an elliptical core [39] is used in form birefringent fibers. A schematic illustration of solid core PM fibers is shown in Fig. 1.5. Due to their solid structure, these PM fibers pose several fundamental limitations, such as material absorption, low damage thresholds, and optical nonlinearity. These limitations have restricted their applications to spectral bands where glass is transparent and to low enough optical power to avoid unwanted nonlinearity and dielectric damage [40]. To counter these limitations, HCFs are ideal candidates that offer low bend losses [41], ultra high bandwidth [42], and high damage threshold [43]. In addition, an NCF design double nested antiresonant nodeless fiber (DNANF) has recently achieved ultra-low loss [31]. Moreover, HCFs offer long propagation lengths for gas-light interaction, enabling interesting new linear and nonlinear applications [44, 45]. Negative curvature hollow-core fibers (NCFs) will remain the focus for polarization preservation throughout this thesis.

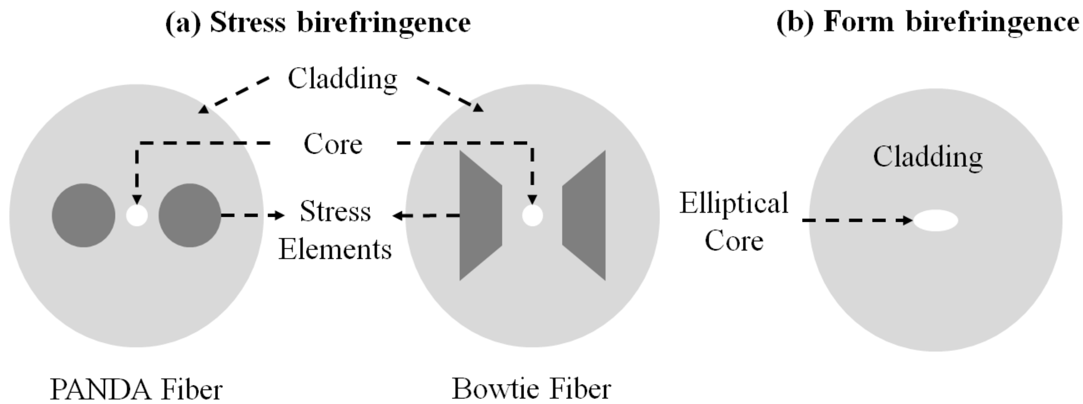

Figure 1.5: Typical solid core PM fibers inducing birefringence through (a) stress and (b) form.

1.2.1 Polarization maintaining negative curvature hollow core fibers (PM-NCFs)

NCFs provide the flexibility to engineer the refractive index of core by introducing various structural configurations using geometry modifications or incorporating different materials, thereby inducing birefringence in the fiber for PM operation. Birefringence is dependent on the light material interaction, and this interaction is found more in solid core fibers. NCFs confine light in the low refractive index air core region, where interactions with the glass inevitably occur. Consequently, as environmental perturbations do not affect air, only the interaction of light with the cladding elements forms the basis for radial asymmetry in the NCFs. These interactions provide a way to introduce birefringence in NCF [46]. However, birefringence in NCFs involves a trade-off between transmission losses, bandwidth, dispersion, and polarization extinction ratio.

The traditional approach of using stress elements to induce birefringence in solid core PM fibers is not applicable in NCFs. Therefore, the core symmetry in NCFs must be broken in different ways for PM operation. A symmetric core NCF consists of uniform material, uniform geometry or microstructure, and circular core resulting in equal effective indices $(N_x = N_y)$ for orthogonal polarizations. Thus, any sort of change to these factors will lead to asymmetric core NCF causing unequal effective indices $(N_x \neq N_y)$ for the orthogonally polarized modes. Fig. 1.6 represents a generic illustration of a uniform simple six-tubular NCF and how an asymmetric core NCF is formed by altering tube thickness t_1 and t_2, cladding tube diameters d_1 and d_2, using elliptical cladding tubes to make elliptical core, application of different materials with refractive indices n_1 and n_2, and using combination of any of these factors. Consequently, birefringence is introduced in NCFs.

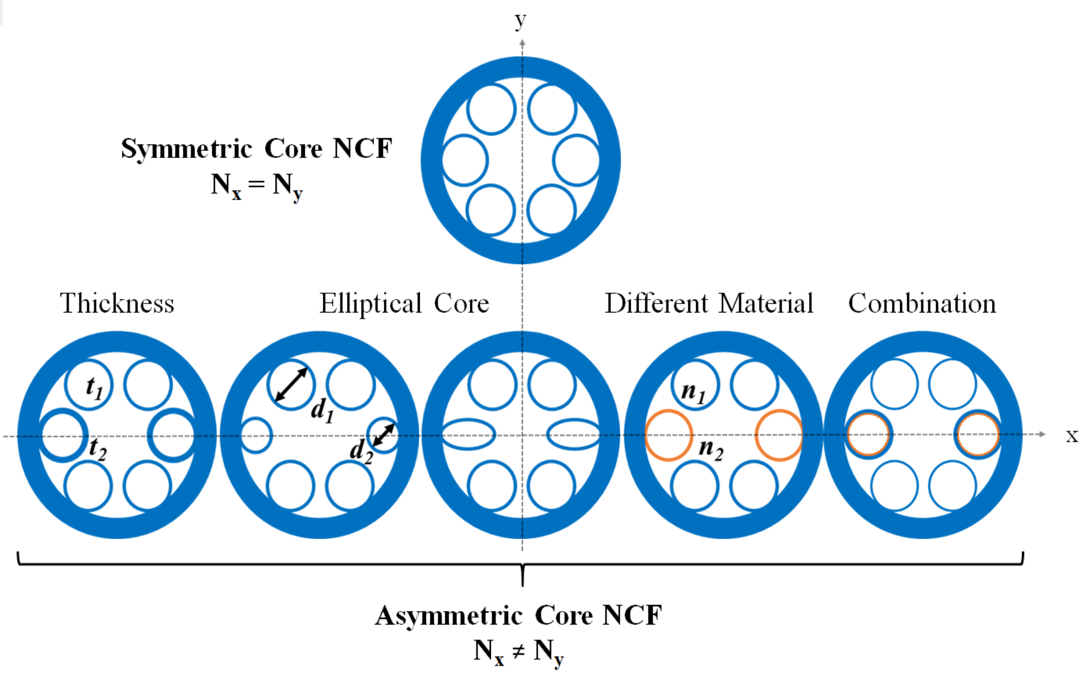

Figure 1.6: A simple six-tube NCF is depicted with a symmetric core and shows how an asymmetric core NCF is produced through variations in orthogonal directions of fiber cross section by using different thicknesses t_1 and t_2, different cladding tube diameters d_1 and d_2, use of elliptical cladding elements to form an elliptical core, applying different material with refractive indices n_1 and n_2, and combination of any of these factors.

One of the first PM-NCF designs used bi-thickness tubes [40]. The use of high refractive index material together with bi-thickness silica tubes has been shown to produce high birefringent PM-NCF [47]. In addition, elliptical cladding elements were employed with strut thickness variations, resulting in high birefringent NCF with low losses for both fundamental modes [48]. Moreover, a semi-circular tube PM-NCF with different silica thicknesses was fabricated, exhibiting strong PM characteristics [49]. These are some of the initial developments in PM-NCFs.

1.3 Objective

A wide range of applications like interferometry, fiber optic gyroscopes, spectroscopy, and fiber sensors essentially require an optical fiber to guide and preserve the input polarization state. While conventional solid-core PM fibers have been in application for a long time, their usage is limited to specific frequency bands and modest optical power due to high material absorption, low damage threshold, and high optical nonlinearity. Negative curvature hollow-core fibers (NCFs) present a viable substitute that can overcome these constraints.

In this thesis, polarization maintaining negative curvature hollow-core fibers (PM-NCFs) are numerically designed and optimized. The research is focused on the following two main objectives;

1. **Enhancing polarization maintenance and spectral filtering in negative curvature hollow-core fibers:** A six-tube PM-NCF design with pole supports is systematically developed for simultaneous polarization maintenance and spectral filtering. The study is focused on achieving polarization and wavelength filtering, maintaining birefringence $\geq 10^{-5}$, and filtered wavelength losses below 0.1 *dB/km*.

2. **Exploring ellipticity effects on polarization maintenance of negative curvature hollow-core fibers:** In this study, a nested tube negative curvature hollow-core fiber is first optimized, and then ellipticity is induced in the whole fiber structure, which makes the core, all cladding tubes and outer tube elliptical with same ellipticity ratio. The polarization-maintaining performance of the fiber is then analyzed in terms of birefringence and polarization extinction ratio.

Chapter 2

Enhancing Polarization Maintenance and Spectral Filtering in Negative Curvature Hollow-Core Fibers

2.1 Introduction

[1]Hollow-core fibers (HCFs) have gained significant attention in the scientific community due to their exceptional properties, such as ultra-low loss transmission, low non-linearity, higher propagation speeds, and high laser-induced damage threshold. Among various types of HCFs, negative curvature hollow-core fibers (NCFs) that possess hypocycloid cladding elements surrounding the core have led to remarkably low transmission losses. NCFs, besides utilizing an anti-resonant reflection mechanism, exhibit inhibited coupling between fundamental core modes and cladding modes due to a mismatch of effective refractive indices together with

[1]The work has been published in Photonics and Nanostructures - Fundamentals and Applications (© 2023 Elsevier) titled "Enhancing polarization maintenance and spectral filtering in negative curvature hollow-core fibers." The author has taken appropriate permission to add the published work to the thesis.

minimum field overlap; thus, they enable efficient light confinement [10]. As a result, NCFs are anticipated to outperform solid-core silica fibers. Although achieving the ultimate goal of ultra-low loss NCF was a challenge, recent advancements in NCF designs based on a double nested tube structure DNANF have shown a transmission loss of 0.174 dB/km in 2022, approaching the lowest loss of solid core fibers across the C-band [30]. With further geometric optimization of DNANF structure, the lowest loss < 0.11 dB/km optical fiber ever is achieved at 1.55 μm [31].

In optical fiber networks, a broad range of frequency bands or wavelength intervals that leverage polarization-dependent properties require a polarized state of light to be preserved, including fiber optic gyroscopes [33], atom spectroscopy [50], optical amplifiers [51], fiber sensors [52, 53], and polarization beam splitters [54, 55]. To conserve and propagate polarized light, polarization-maintaining (PM) fibers are intentionally designed with an asymmetric core by introducing either different materials or geometry to obtain birefringence between two orthogonal fundamental modes (FM). However, introducing birefringence in PM-NCFs requires alternative approaches since the birefringence mechanism in conventional solid core PM fibers, like the use of stress rods, is not applicable to NCF. One of the initial PM-NCF designs employed a bi-thickness tube structure to achieve high birefringence [40]. Over the years, PM-NCF designs and structures have progressed by the adoption of the anisotropic core through microstructures, elliptical cores, the addition of high-refractive-index cladding elements, or combinations thereof [47, 48, 56, 57].

Frequency-selective transmission in optical fibers is desired for applications in optical communication, sensing, and lasers, and it is mainly studied in solid-core fibers. Fiber bandpass filters find widespread use in wavelength division multiplexing (WDM) optical communication systems [58], temperature & pressure sensors are built based on fiber Bragg gratings (FBG) [59, 60], chirped fiber Bragg gratings (CFBGs) which are modified FBGs serve as optical pulse generators [61], and photonic crystal fibers (PCFs) have been employed for multi-wavelength lasing application in erbium-doped fiber lasers [62]. However, the spectral filtering capabilities in NCFs still remain unexplored.

In this study, a systematic development of a novel polarization maintaining and spectral filtering NCF design is presented. The designed six-tube silica PM-NCF supported with pole structure exhibits a wavelength selective transmission loss profile specifically for the vertically polarized state, attributed to the presence of pole structure that radially positions the nested tube in the vertical direction, while nested tubes without a pole structure are utilized in the horizontal direction. The filtered wavelengths demonstrate transmission losses below 0.1 dB/km, accompanied by a birefringence level $\geq 10^{-5}$. These results represent significant improvements compared to previously reported findings [63, 64]. The optimized fiber offers a bandwidth of 150 nm, an improved polarization extinction ratio, and a reduced number of spectrally filtered wavelengths. The proposed fiber design holds considerable potential for applications that require simultaneous polarization maintenance and spectral filtering.

2.2 Fiber design and simulation method

The cross-sectional schematic of the proposed pole-supported nested tubular polarization maintaining NCF (P-PMNCF) structure is depicted in Fig. 2.1a. The P-PMNCF structure is designed with silica glass and incorporates a pole NCF structure (Fig. 2.1b) in the vertical direction, while an NT-NCF structure (Fig. 2.1c) is presented in the horizontal axis to generate two orthogonal polarization states. The designed fiber features a six-tube structure with a core diameter, D. The outer cladding tubes have a thickness, t_2, in the horizontal direction, while all the remaining cladding elements have a uniform thickness, t_1. The inclusion of different cladding tube thicknesses in the horizontal and vertical axes is essential to induce high birefringence, which is a key requirement for a PM fiber. The outer cladding tubes' diameter is denoted as d_1, while the nested tubes' diameters in the horizontal and vertical directions as d_2 and d_3, respectively. The pole length, L_p, controls d_3 according to the following relation:

$$d_3 = d_1 - 2L_p - 2t_1 \tag{2.1}$$

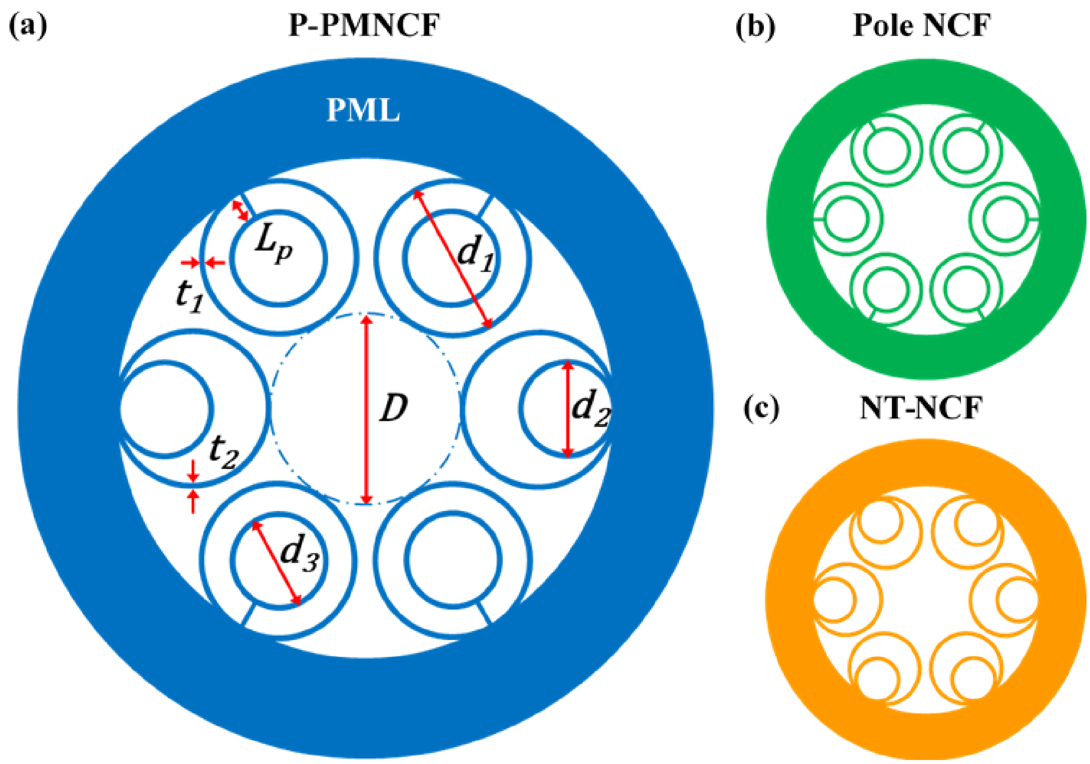

Figure 2.1: (a) Cross-sectional schematic of pole supported nested tubular polarization-maintaining NCF (P-PMNCF) structure, showing the core diameter, D; outer cladding tubes' diameter, d_1; nested cladding tubes' diameter in the horizontal and vertical axes, d_2 and d_3, respectively. The thickness of outer cladding tubes in the horizontal and vertical directions, t_2 and t_1, respectively; and the pole length, L_p. Design of (b) the pole-linked negative curvature fiber (Pole-NCF) and (c) the nested tube negative curvature fiber (NT-NCF).

The numerical simulations were performed based on a finite element-based electromagnetic wave frequency domain (EWFD) solver in COMSOL Multiphysics in a two-dimensional space. To execute numerical studies in COMSOL, the refractive index was defined in the electric displacement field. Since air is regarded as a non-dispersive medium, all studies employed a constant refractive index of 1. Silica is implemented as a cladding material. Only the real part of the wavelength-dependent refractive index for silica is employed for confinement loss calculations since material absorption and surface scattering losses have a negligible contribution to the performance of the NCFs in near-IR region [65, 66]. In order to achieve accurate results, necessary boundary conditions were used for the fiber. A perfectly matched layer (PML) was applied at the outer cladding region to reduce the computational power of simulations [67]. Whereas at the outer perimeter of the fiber, a scattering boundary condition was employed. PM-NCF does not have a symmetric core in terms of effective refractive index; therefore, the full geometry of the fiber was used every time for simulations.

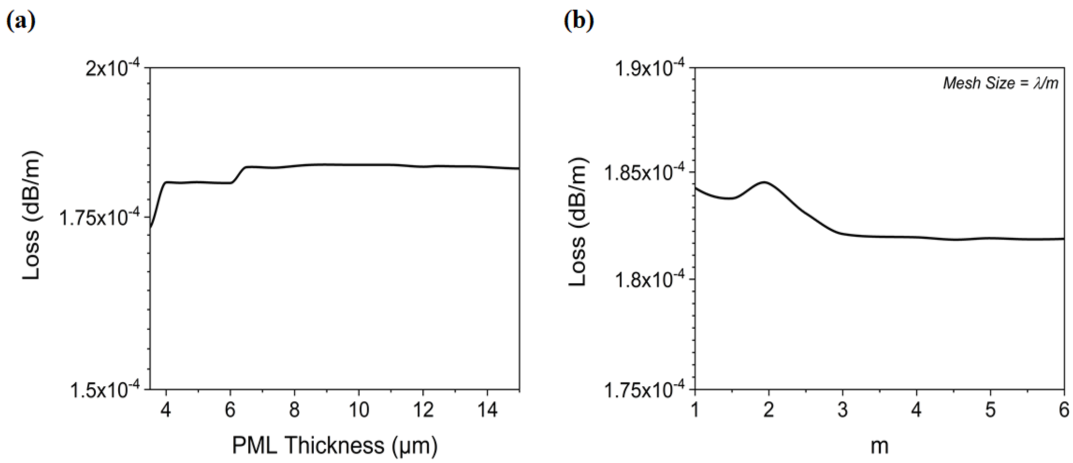

Figure 2.2: Convergence studies for (a) the PML thickness and (b) the mesh size parameter m.

Initially, convergence studies were carried out to optimize the mesh size and thickness of perfectly matched layers (PMLs) for precise and valid results. Through these studies, the optimum thickness of PML was found to be 10 μm while the optimized maximum mesh size $\lambda/4$ was determined, ensuring that narrow regions of the cladding contained a minimum of five elements. The effect of PML thickness and mesh parameter m on confinement loss is shown in Fig. 2.2(a) and Fig. 2.2(b), respectively.

Birefringence, one of the most important characteristics of PM Fibers, can be calculated as [47]:

$$B = |N_H - N_V| \tag{2.2}$$

where N_H and N_V are the effective refractive indices for horizontal and vertical polarization states, respectively.

The confinement loss is a dominant loss mechanism in the near-IR region for silica NCF, which is calculated by the following formula in decibels per meter (dB/m) [47]:

$$L_c = 8.686 \times \left(\frac{2\pi}{\lambda}\right) \times I_{imagine}(N_{eff}) \tag{2.3}$$

where $I_{imagine}$ is the imaginary part of effective refractive index (N_{eff}) and λ is the wavelength of operation in μm.

The thickness, t_1, is already optimized in our earlier studies for the targeted spectral region [63, 64]. In this study, we focus on optimizing the structural parameters, namely t_2, d_2, L_p and D to achieve a target transmission loss below 0.1 *dB/km* for the spectrally filtered wavelengths, while maintaining a birefringence level exceeding 10^{-5}.

2.3 Results and discussions

2.3.1 Optimization of wall thickness (t_2)

The study was initiated by analyzing the effect of cladding tube thickness, t_2, on the fiber performance at the wavelength vicinity of 1.55 μm, with parameters $D = 30\,\mu m$, $t_1 = 0.4\,\mu m$, $d_1 = 25\,\mu m$, $d_2 = 15\,\mu m$, and $L_p = 4.6\,\mu m$. Fig. 2.3(a) and Fig. 2.3(b) illustrate the impact of varying wall thickness, t_2, on confinement loss and birefringence, respectively. As shown in Fig. 2.3(a), the vertical polarization loss exhibits a range of t_2 values with confinement losses below 0.1 *dB/km*, reaching the lowest loss when t_2 equals $t_1 = 0.4\,\mu m$, while horizontal polarization experiences higher losses. Moving to the larger thickness values towards the resonance region from this point, the losses gradually increase. Further, Fig. 2.3(b) demonstrates an increasing trend in birefringence as t_2 approaches the resonance points. To achieve high birefringence and target losses for vertical polarization, it is necessary to set t_2 closer to the resonance region.

To further explore the confinement losses and birefringence over the wavelength spectrum, parametric sweeps were performed for t_2 ranging from 0.55 μm to 0.66 μm. Contour plots shown in Fig. 2.3(c), Fig. 2.3(d), and Fig. 2.3(e)

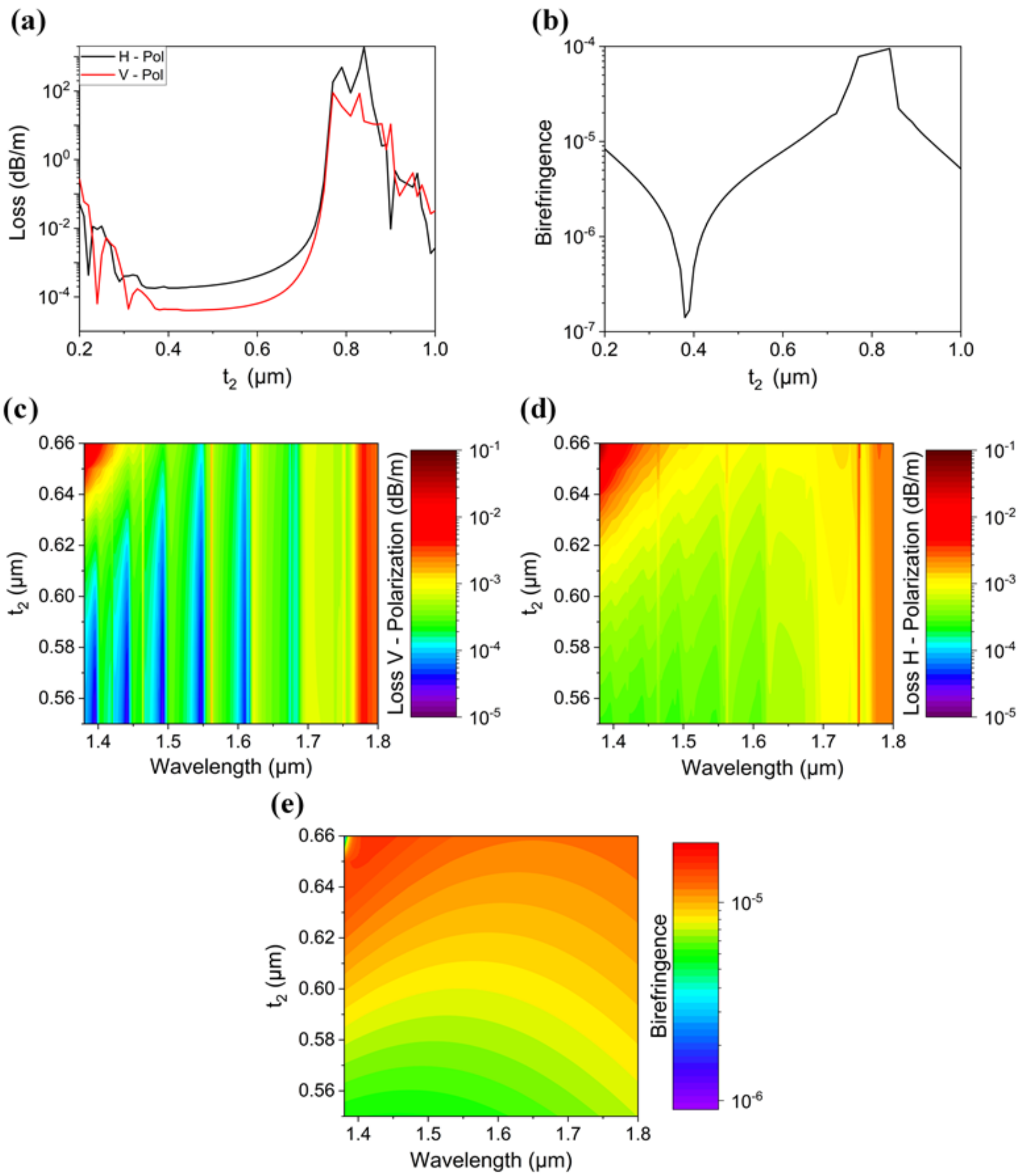

Figure 2.3: (a) Impact of t_2 on the confinement loss of horizontally (H) and vertically (V) polarized states at 1.55 μm wavelength. (b) Impact of t_2 on birefringence at 1.55 μm wavelength. (c) Contour plot of vertical polarization (V) loss from 1.38 μm to 1.8 μm wavelength spectrum as a function of t_2. (d) Contour plot of horizontal polarization (H) loss from 1.38 μm to 1.8 μm wavelength spectrum as a function of t_2. (e) Contour plot of birefringence from 1.38 μm to 1.8 μm wavelength spectrum as a function of t_2.

depict these parametric sweeps. Fig. 2.3(c) illustrates the characteristic spectral filtering regions with alternating low and high loss regions for the vertical polarization. The dark blue regions represent the filtered wavelengths, exhibiting losses below the threshold of 0.1 *dB/km*. Conversely, Fig. 2.3(d) demonstrates high losses ($\geq 10^{-5}$) for the horizontal polarization. Increasing t_2 reduces the number of filtered wavelengths as the resonance points shift towards $1.55\,\mu m$ wavelength as demonstrated in Fig. 2.3(c). Simultaneously, the birefringence of the fiber increases, as shown in Fig. 2.3(e). The optimum thickness, $t_2 = 0.62\,\mu m$, was found after careful evaluation, resulting in three filtered wavelength ranges: 1.488–1.494 μm, 1.542–1.550 μm, and 1.604–1.612 μm, while maintaining birefringence in close proximity to 10^{-5}.

2.3.2 Optimization of nested tube diameter (d_2)

In pursuit of achieving the lowest vertical polarization losses for filtered wavelengths, high horizontal polarization losses, and high birefringence, the fiber performance was investigated using the effect of nested tube diameter, d_2. A parametric sweep on d_2 was run at a wavelength of $1.55\,\mu m$ using the fiber parameters: $D = 30\,\mu m$, $t_1 = 0.4\,\mu m$, $d_1 = 25\,\mu m$, $t_2 = 0.62\,\mu m$, and $L_p = 4.6\,\mu m$. Fig. 2.4(a) and Fig. 2.4(b) depict the behavior of confinement loss and birefringence of the fiber, respectively, as d_2 varies. As shown in Fig. 2.4(a), increasing d_2 leads to the attainment of minima in the confinement losses, with the horizontal polarization loss reaching its minimum ahead of the vertical polarization loss. This observation suggests that by moving to the right from the point of lowest horizontal loss, it is possible to achieve simultaneous vertical polarization losses below 0.1 *dB/km* and higher horizontal polarization losses exceeding 1 *dB/km*, ensuring a high polarization extinction ratio for PM operation. Additionally, Fig. 2.4(b) demonstrates that birefringence gradually decreases with increasing d_2 and then abruptly reduces near the resonance points on the right.

The behavior of confinement losses and birefringence was examined over a wavelength range of $1.3\,\mu m$ to $1.8\,\mu m$, by varying d_2 from $13\,\mu m$ to $19\,\mu m$, based

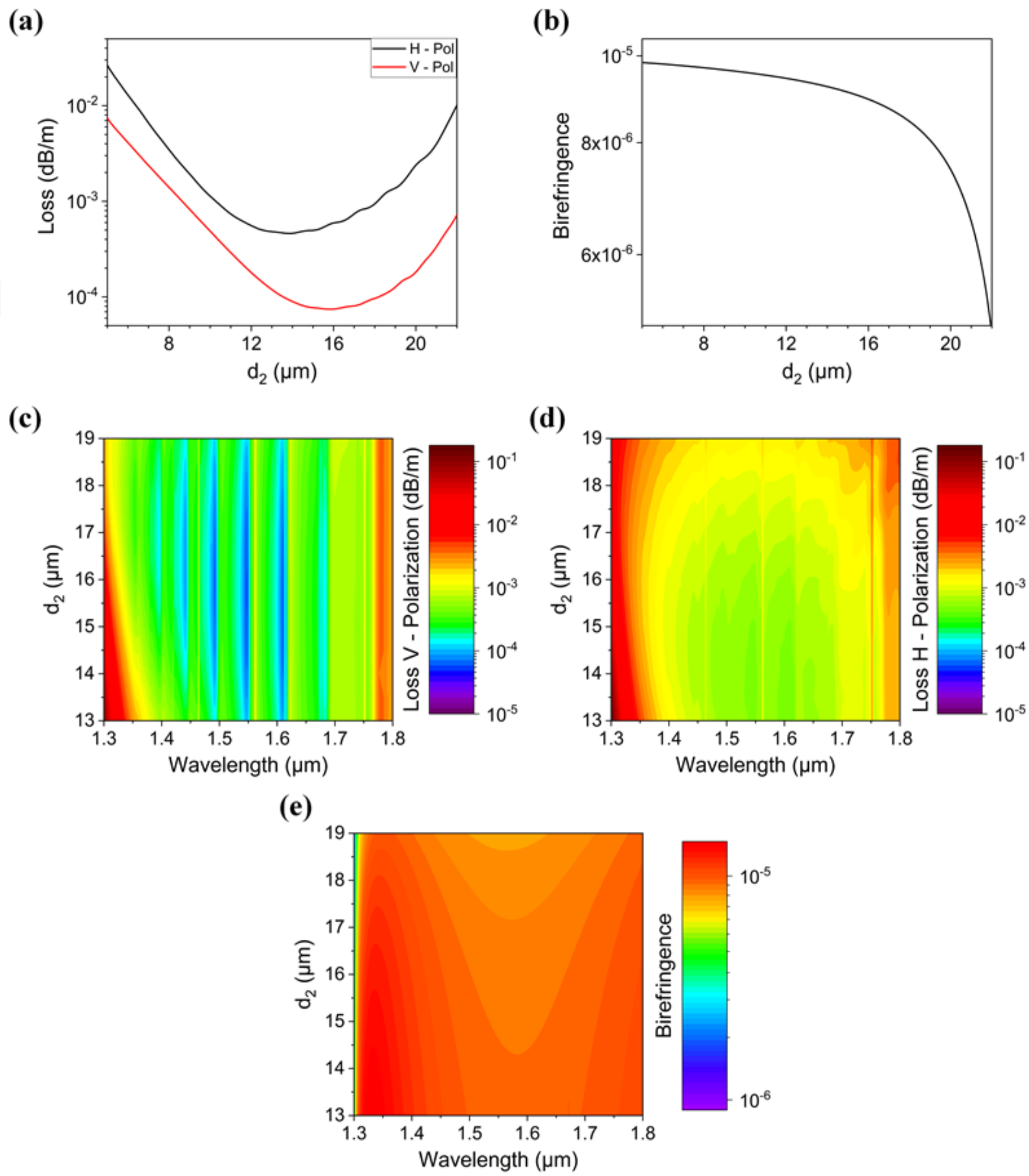

Figure 2.4: (a) Impact of d_2 on the confinement loss of horizontally (H) and vertically (V) polarized states at $1.55\,\mu m$ wavelength. (b) Impact of d_2 on birefringence at $1.55\,\mu m$ wavelength. (c) Contour plot of vertical polarization (V) loss from $1.3\,\mu m$ to $1.8\,\mu m$ wavelength spectrum as a function of d_2 (d) Contour plot of horizontal polarization (H) loss from $1.3\,\mu m$ to $1.8\,\mu m$ wavelength spectrum as a function of d_2. (e) Contour plot of birefringence from $1.3\,\mu m$ to $1.8\,\mu m$ wavelength spectrum as a function of d_2.

on insights gained from Fig. 2.4(a) and Fig. 2.4(b). Contour plots for confinement loss, shown in Fig. 2.4(c) and Fig. 2.4(d), corroborate the findings of Fig. 2.4(a), but now considering a constant wavelength region. Progressing in the longer wavelength direction, three distinct regions of selective transmission with losses below the target for vertical polarization are observed in Fig. 2.4(c). On the other hand, when moving along the vertical axis within the filtered wavelength region, it can be seen that the losses reach a minimum at $d_2 = 16\,\mu m$, and then start to increase again, exceeding 0.1 dB/km at $d_2 = 19\,\mu m$. Fig. 2.4(d), the contour plot for horizontal polarization loss, assists in determining the optimum d_2 level. It is found that higher values of d_2 enable us to achieve the highest possible horizontal polarization loss while maintaining the vertical polarization loss for filtered wavelengths below 0.1 dB/km. Although the overall birefringence (see Fig. 2.4(e)) decreases with larger d_2 values, but the change is not significant. After careful consideration, $d_2 = 18\,\mu m$ was finalized, which allows us to achieve the desired losses and birefringence close to the target for further examination of P-PMNCF design.

2.3.3 Optimization of pole length (L_p)

To delve deeper into fiber characterization, the effect of pole length, L_p, on confinement loss and birefringence was explored. The parametric sweep was run for L_p at $1.55\,\mu m$ wavelength with fiber parameters $D = 30\,\mu m$, $t_1 = 0.4\,\mu m$, $d_1 = 25\,\mu m$, $t_2 = 0.62\,\mu m$, and $d_2 = 18\,\mu m$. The effect of L_p on confinement loss and birefringence is shown in Fig. 2.5(a) and Fig. 2.5(b), respectively. The vertically polarized state shows alternate high and low loss regions featuring a spectral filter, which is different from the horizontally polarized state loss profile as illustrated in Fig. 2.5(a). This observation proves that frequency selective transmission characteristic for vertical polarization of P-PMNCF is due to the pole anchors. In Fig. 2.5(a), as L_p is increased the filtered wavelength is shifting to the right. The filtered wavelengths close to the resonance regions show higher losses, while those residing in the anti-resonance region display the lowest losses.

Nine different ranges of pole length were found for filtered wavelengths bearing losses below 0.1 dB/km; A: 3.45–3.47 μm, B: 4–4.04 μm, C: 4.54–4.6 μm, D: 5.12–5.16 μm, E: 5.66–5.72 μm, F: 6.2–6.27 μm, G: 6.78–6.82 μm, H: 7.34–7.36 μm, and I: 7.88–7.9 μm. The lowest loss points of L_p among each of these ranges were selected to run a wavelength sweep in order to further inspect the effect of pole length on confinement loss over the wavelength spectrum. The trend of confinement loss over wavelength spectrum can be easily understood with three L_p values (A) 3.46 μm, (E) 5.7 μm and (I) 7.89 μm as depicted in Fig. 2.5(c), Fig. 2.5(d) and Fig. 2.5(e). The filtered wavelength spectrum for vertical polarization loss is narrower for 3.46 μm and broader for 7.89 μm, suggesting that the filtered wavelength spectrum is broadening as pole length is increased. Moreover, the pole lengths 3.46 μm and 7.89 μm show high vertical polarization losses as compared to 5.7 μm while horizontal polarization losses do not have any noticeable change. On the other hand, Fig. 2.5(b) shows a declining effect on birefringence as pole length is increased. This outcome is well supported by Fig. 2.5(f) which shows birefringence behavior over wavelength sweep for pole lengths (A) 3.46 μm, (E) 5.7 μm and (I) 7.89 μm showing the highest birefringence over the wavelength spectrum for 3.46 μm while the lowest birefringence is observed for 7.89 μm pole length. The decrease in birefringence is not very significant. After analysis, we found $L_p = 5.7\,\mu m$ as the optimum point, which has the lowest filtered wavelength losses below 0.1 dB/km for vertical polarization with broad filtered spectrum while the birefringence is lower but still close to 10^{-5}.

2.3.4 Optimization of core diameter (D) and core ellipticity (D_x)

Reduction in core size increases the confinement loss and birefringence [40]. Thus, a trade-off is required in order to achieve desired birefringence with acceptable loss levels. Fig. 2.6a illustrates the effect of changing core diameter D on confinement loss and birefringence at 1.55 μm wavelength with fiber structure $t_1 = 0.4\,\mu m$, $d_1 = 25\,\mu m$, $t_2 = 0.62\,\mu m$, $d_2 = 18\,\mu m$ and $L_p = 5.7\,\mu m$. It is evident from Fig. 2.6(a) as the core diameter is decreasing, confinement losses for both polarizations and

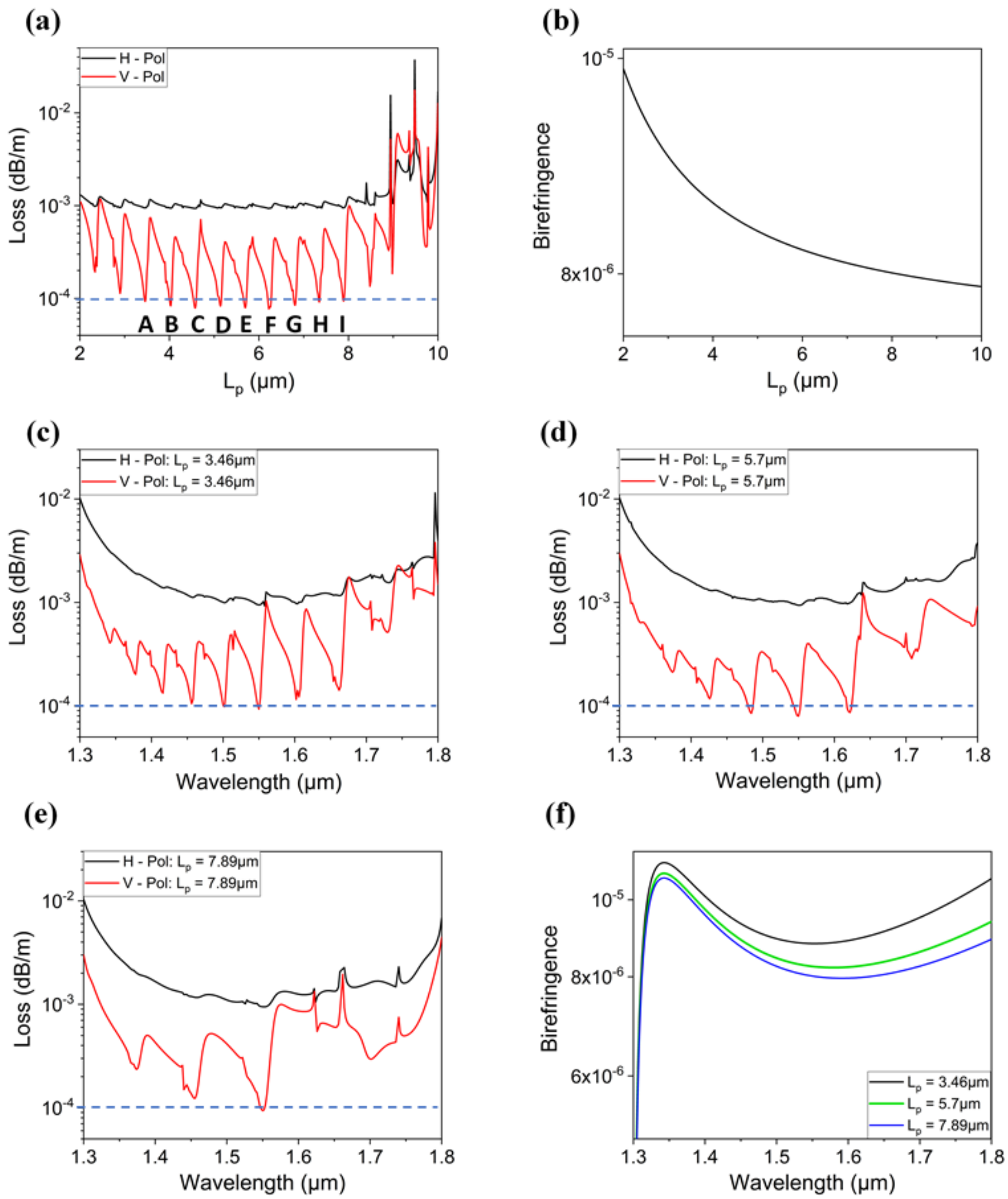

Figure 2.5: (a) Impact of L_p on the confinement loss of horizontally (H) and vertically (V) polarized states, nine ranges of L_p (A to I) showing filtered wavelength losses below the threshold at 1.55 μm wavelength, (b) impact of L_p on birefringence at 1.55 μm wavelength, (c) confinement losses at $L_p = 3.46\,\mu m$ from 1.3 μm to 1.8 μm wavelength spectrum, (d) confinement losses at $L_p = 5.7\,\mu m$ from 1.3 μm to 1.8 μm wavelength spectrum, (e) confinement losses at $L_p = 7.89\,\mu m$ from 1.3 μm to 1.8 μm wavelength spectrum, and (f) birefringence from 1.3 μm to 1.8 μm wavelength spectrum.

birefringence are increasing. In order to have losses below 0.1 *dB/km* for filtered wavelengths in vertically polarized state, the D value needs to move to the right of 29 μm while to achieve birefringence in 10^{-5} range, the value of D needs to travel to the left of 28.15 μm. So, the targets for filtered wavelength losses and birefringence cannot be met simultaneously by reducing the core diameter. Then, ellipticity was introduced in the fiber keeping D_y constant at 30 μm and changing D_x as demonstrated in Fig. 2.6(b). The fiber has a circular core at $D_x = 30\,\mu m$ and as it is moved to the smaller values more and more ellipticity is induced in the fiber core. Since D_y is kept constant and D_x is decreasing, the losses for vertically polarized state are shifted down as compared to the impact of decreasing core diameter in Fig. 2.6(a). Therefore, a range of D_x from 27 μm to 28.45 μm gives the desired filtered wavelength losses and birefringence as evident in Fig. 2.6(b).

Parametric wavelength sweeps were run using D_x 27 μm, 27.75 μm, 28.45 μm and 30 μm for confinement losses and birefringence as presented in Fig. 2.6(c) and Fig. 2.6(d), respectively. Fig. 2.6(c) shows as D_x value is dropped from 30 μm, the resonance points on the longer wavelength side for vertical polarization are moving to the smaller wavelength values towards 1.55 μm wavelength. As a result, the filtered wavelengths are reduced from three (when the core was circular) to two with losses below 0.1 *dB/km*. Further, the operational bandwidth is reduced to 1.45–1.60 μm. Moreover, the birefringence of the fiber is shifted upwards above 10^{-5} if more ellipticity is introduced in the fiber as demonstrated in Fig. 2.6(d). The optimum value of D_x is selected as 27.75 μm with two filtered wavelength ranges; 1.482–1.486 μm and 1.546–1.552 μm having birefringence above but again still close to 10^{-5}.

Considering that the P-PMNCF fiber was designed on three fundamental criteria, including having the PM property with spectral filtering ability, keeping the birefringence above 10^{-5}, and filtered wavelength losses below 0.1 *dB/km*. So, with the proposed structure, the initial goals were simultaneously achieved, but having the birefringence in the range of 10^{-4} while preserving the other parameters was highly challenging. Therefore, the target for the birefringence was maintained at 10^{-5}.

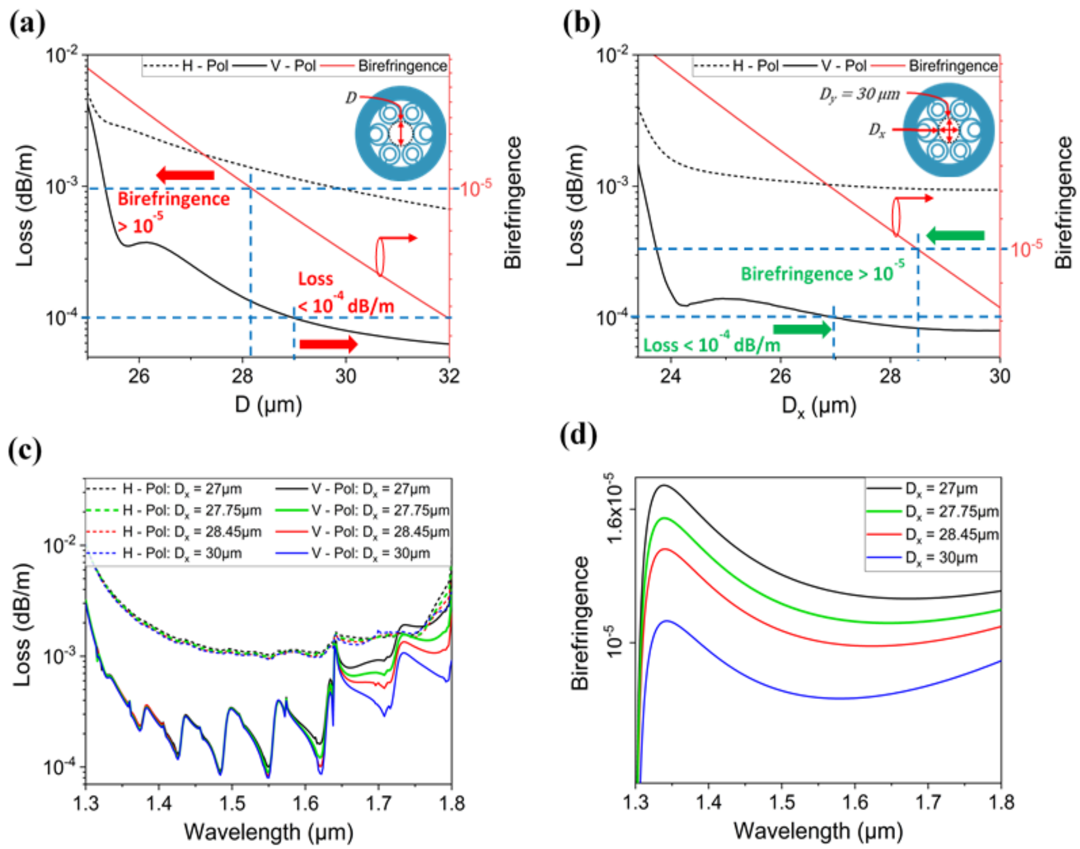

Figure 2.6: (a) Impact of core diameter D on confinement losses (horizontal polarization – H and vertical polarization – V) and birefringence at $1.55\,\mu m$ wavelength, (b) effect of core ellipticity D_x on confinement losses (horizontal polarization – H and vertical polarization – V) and birefringence at $1.55\,\mu m$ wavelength, (c) confinement loss profiles with respect to D_x from $1.3\,\mu m$ to $1.8\,\mu m$ wavelength spectrum, and (d) birefringence with respect to D_x from $1.3\,\mu m$ to $1.8\,\mu m$ wavelength spectrum.

2.4 Spectral filtering

The alternate high and low loss regions observed in the vertically polarized state of P-PMNCF fiber can be described as frequency-selective transmission, as shown in Fig. 2.6(c). The minima in the loss profile represent filtered wavelengths with low losses, while the maxima signify unfiltered wavelengths with high losses. The selective transmission effect is due to the presence of pole anchors aligned along the vertical axis. Within this unique transmission spectrum, the high-loss regions result from light coupling with the pole anchors, while there is no light coupling in the low-loss regions. Therefore, P-PMNCF fiber shows distinct spectral filtering patterns of fluctuating high and low loss zones exclusively for vertical polarization, and this phenomenon is directly attributed to the presence of pole anchors positioned in the vertical direction [63, 64].

2.5 Fabrication feasibility

The fabrication of P-PMNCF fiber will be a highly challenging process, especially considering the anchored pole structure of the fiber, but it may be realized using the stack and draw method. There will be several distinct steps in the fabrication method. First, the preform for the vertical cladding elements with pole anchor can be stacked using the tubes and flat pieces with the help of small support capillaries. This preform then undergoes a thermal drawing process in a fiber draw tower to attain the requisite dimensions for the final stacking of the fiber preform. Similarly, the same sequence can be used to produce the preform for horizontal cladding elements without pole anchors using tubes and small support capillaries. Finally, all prepared cladding elements (four cladding tubes with pole-anchored nested tubes and two cladding tubes with standard nested tubes) can be stacked together to prepare the final preform. Subsequently, the fiber can be drawn in a draw tower using the preform under high temperatures around the working range of the silica glass. However, practically achieving the proposed fiber will take a lot of effort, and may require a comprehensive fabrication study.

Chapter 3

Exploring Ellipticity Effects on Polarization Maintenance of Negative Curvature Hollow-Core Fibers

3.1 Introduction

One of the ways to introduce high birefringence in conventional solid-core PM fibers is by making the core elliptical [39]. However, using ellipticity in PM-NCFs does not produce effective results [40]. Meanwhile, elliptical cladding elements were used together with circular tubes, making the core elliptical to produce high birefringence with low transmission losses for both orthogonal polarization modes [48]. The impact of ellipticity on polarization maintaining performance of PM-NCFs has not been thoroughly studied.

This chapter is dedicated to investigating the polarization-maintaining properties of PM-NCFs under the effect of ellipticity. A six-tube silica nested tube negative curvature fiber (NT-NCF) is first optimized. Afterward, the whole NT-NCF structure is subjected to ellipticity, which causes an anisotropic core to be formed in the fiber. Consequently, the fiber generates two orthogonal polarization states capable of preserving the input state of polarization.

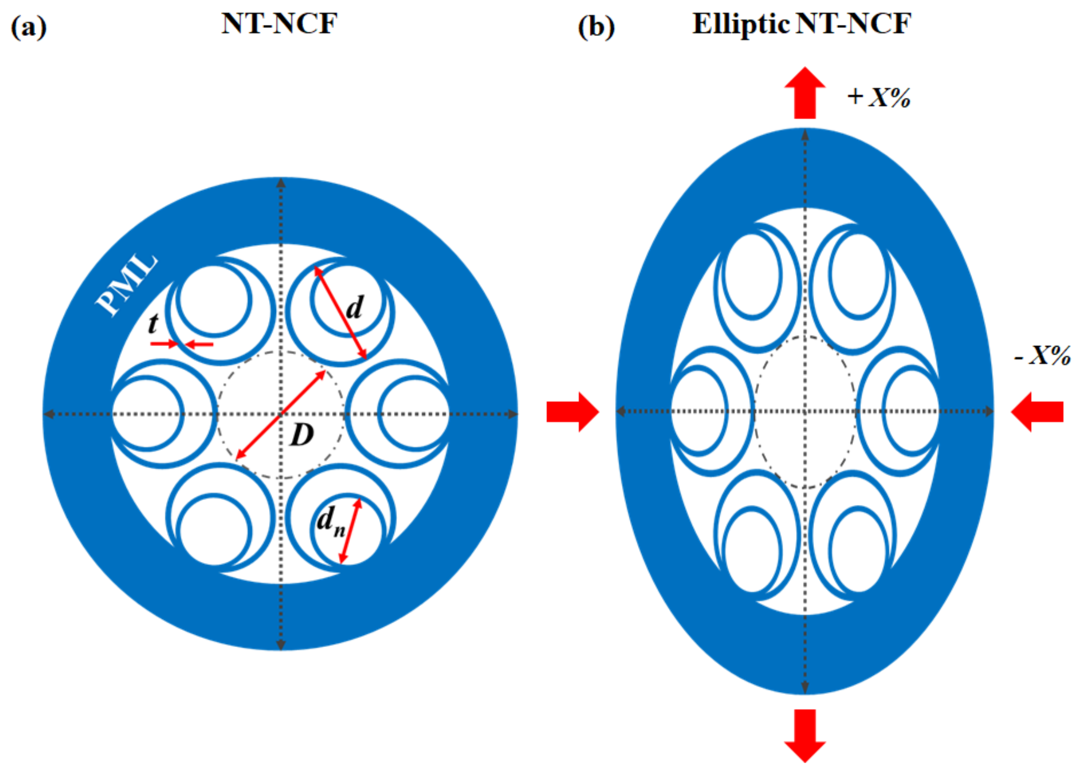

Figure 3.1: (a) Cross-sectional schematic of nested tube negative curvature fiber (NT-NCF), showing the core diameter, D, outer cladding tubes' diameter, d, nested cladding tubes' diameter, d_n, and the thickness of all cladding tubes', t, and (b) design of elliptic NT-NCF, when NT-NCF is elongated by $+X\%$ and contracted by $-X\%$ in the vertical and horizontal directions, respectively. The whole fiber structure, including the core, all the cladding tubes, and the outer jacket, becomes elliptical.

3.2 Fiber design and methodology

The non-PM nested tube negative curvature fiber (NT-NCF) is illustrated in Fig. 3.1(a). The fiber employs a six-tube geometry with a core diameter, D, strut thickness, t, outer cladding tubes' diameter, d, and nested tubes' diameter,

d_n. When this fiber undergoes elongation and contraction in the vertical and horizontal axes, respectively, with the same ellipticity ratio ($X\%$), the core, all the cladding tubes, and the outer fiber jacket of NT-NCF become elliptical. Therefore, an Elliptic NT-NCF structure is formed, as shown in Fig. 3.1(b), capable of PM operation.

In COMSOL Multiphysics, the electromagnetic wave frequency domain (EWFD) solver based on the finite element method was used for numerical studies. The simulation methodology is similar to as described in the section 2.2. After running the convergence studies for PML thickness and mesh optimization, the geometry of NT-NCF with a core diameter, $D = 30\,\mu m$ was fine-tuned at $1.55\,\mu m$.

Birefringence and confinement loss are calculated using equations 2.2 and 2.3, respectively. Meanwhile, the polarization extinction ratio (PER) is defined as the ratio of the loss of unwanted polarization to the loss of desired polarization [47].

$$\text{PER} = \frac{\text{Horizontal polarization loss}}{\text{Vertical polarization loss}} \tag{3.1}$$

3.3 Results and discussion

3.3.1 Ellipticity effect on NT-NCF

Through parametric studies, the NT-NCF structure (Fig. 3.1(a)) was optimized with parameters $t = 0.41\,\mu m$, $d = 0.85D$, and $d_n = 0.56d$ at $1.55\,\mu m$. The confinement loss profile of NT-NCF is shown in Fig. 3.2(a) for a wavelength spectrum $0.9\,\mu m$ to $1.9\,\mu m$. This fiber with the isotropic core cannot achieve PM operation. With the introduction of the ellipticity of 5%, 8%, and 10% in NT-NCF, the fiber exhibited vertical polarization (V) and horizontal polarization (H) states as shown in Fig. 3.2(b). With the increase in ellipticity, both polarization states experienced higher losses. Additionally, there was also a shift of resonance points from high wavelength to low wavelength regions with increasing ellipticity. Consequently, the bandwidth of the elliptic NT-NCF was reduced with 10% ellipticity showing the smallest bandwidth while 5% ellipticity had the largest bandwidth, as depicted in Fig. 3.2(b). Introducing more than 10% ellipticity was unsuitable since the fiber geometry collapsed during numerical studies.

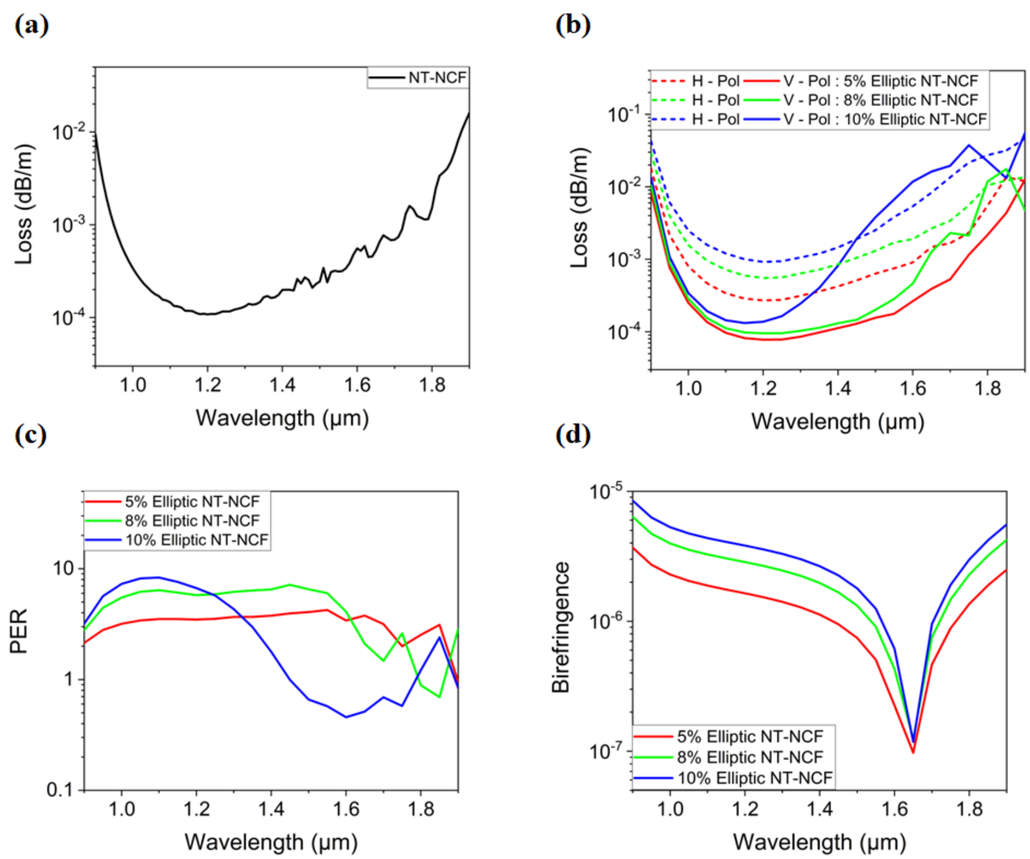

Figure 3.2: (a) Confinement loss of nested tube negative curvature fiber (NT-NCF) from 0.9 μm to 1.9 μm wavelength spectrum, (b) confinement loss of vertically (V) and horizontally (H) polarized states, (c) polarization extinction ratio (PER), and (d) birefringence at 5%, 8%, and 10% ellipticity from 0.9 μm to 1.9 μm wavelength spectrum.

The PER of the elliptic NT-NCF experienced an increasing trend with larger ellipticity values as illustrated in Fig. 3.2(c). Due to the lowest bandwidth for 10% elliptic NT-NCF, the PER was first highest till 1.2 μm wavelength and then decreased to the lowest PER values. In the context of broader bandwidth 8% elliptic NT-NCF exhibited better PER. Overall, the PER was lower than 10 which is not enough for optimal performance. For a sufficiently long birefringent fiber, the PER of > 100 is desired to remove any unwanted cross-coupled polarization [47]. Fig. 3.2(d) shows the effect of ellipticity on fiber birefringence. With increasing ellipticity, the birefringence was getting higher. At a constant ellipticity, the birefringence first decreased with increasing wavelength values, reaching a minimum point at around $1.65\,\mu m$ and then followed an increasing trend at larger wavelengths. The minimum of birefringence was due to the effective indices of vertical (N_V) and horizontal (N_H) polarizations, which approached each other at $1.65\,\mu m$. The highest birefringence is in the range of 10^{-6}, which is very low compared to commercial PM fibers having birefringence $> 10^{-4}$. In the subsequent sections, the effect of 8% ellipticity will be analysed due to its broader bandwidth and fairly better PER and birefringence.

3.3.2 Bi-thickness effect coupled with ellipticity

Bi-thickness was introduced in the NT-NCF design with a thickness t_2 along the horizontal axis of the fiber on outer cladding tubes as illustrated in Fig. 3.3(a) while keeping all other parameters constant at $D = 30\,\mu m$, $d = 0.85D$, $d_n = 0.56d$ and t became $t_1 = 0.41\,\mu m$. Through parametric sweep at $1.55\,\mu m$ wavelength, $t_2 = 0.65\,\mu m$ was selected for further analysis due to better birefringence with low confinement losses. Orthogonal polarization modes were generated for NT-NCF design due to the presence of t_2 thickness as depicted in the confinement loss curve in Fig. 3.3(c), in contrast to the the initial state of NT-NCF, where single strut thickness $t_1 = t_2 = 0.41\,\mu m$ was used. Further, there was a shift of resonance points from low wavelength to higher wavelength values, which resulted in reduced bandwidth for NT-NCF with bi-thickness compared to original NT-NCF design, as observed in Fig. 3.3(c).

Moreover, from Fig. 3.3(c), it can be seen that the elliptic NT-NCF with 8% ellipticity and bi-thickness experienced higher losses for both polarization states than NT-NCF with only bi-thickness. In addition, the resonance points in 8% elliptic NT-NCF with bi-thickness have moved from higher to lower spectral

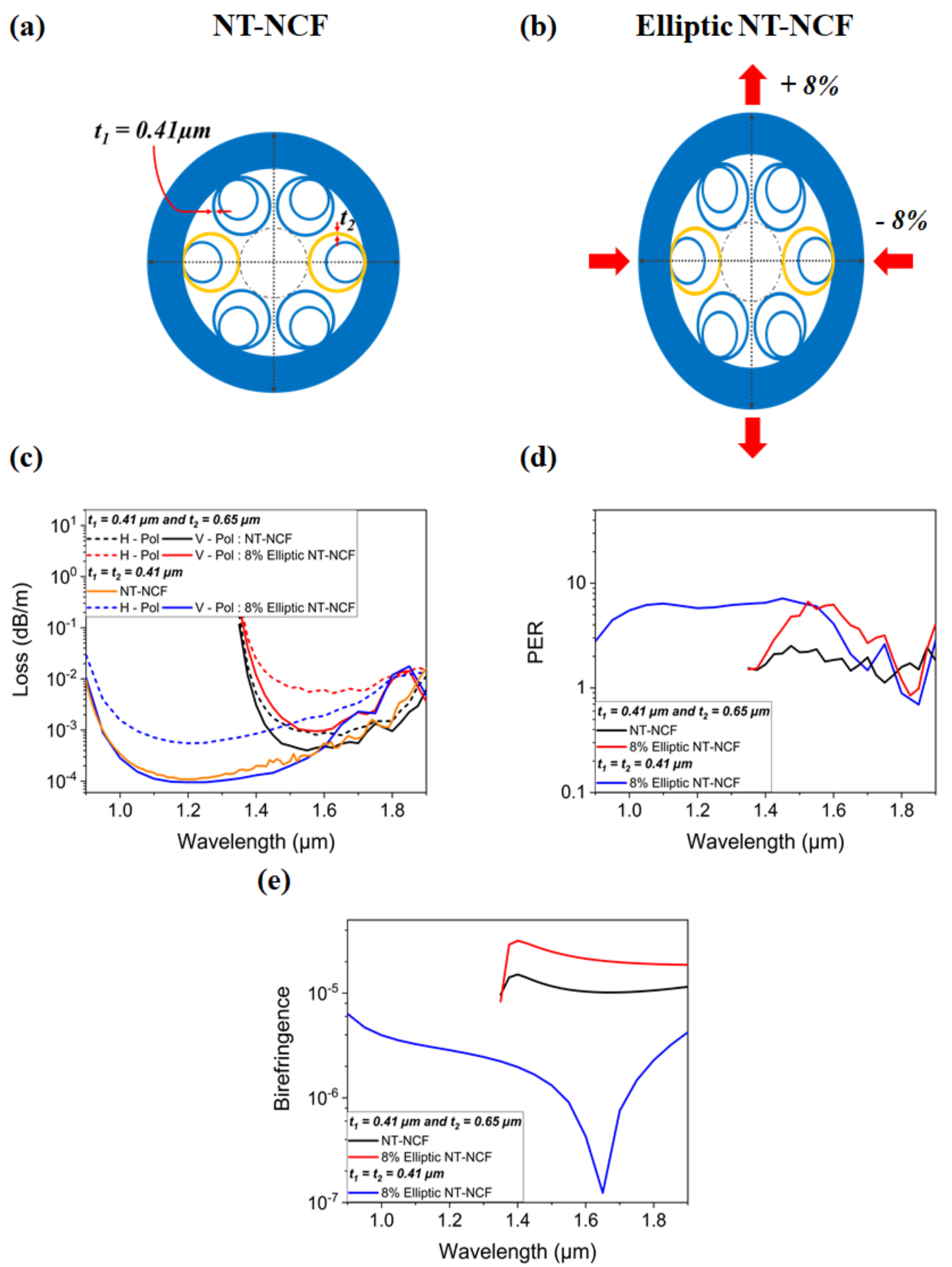

Figure 3.3: Schematic illustration of the implementation of thickness t_2 on outer cladding tubes along the horizontal direction in (a) NT-NCF design and (b) 8% elliptic NT-NCF design, (c) confinement loss comparison, (d) PER comparison, and (e) birefringence comparison between NT-NCF and 8% elliptic NT-NCF designs with and without t_2 thickness implementation from $0.9\,\mu m$ to $1.9\,\mu m$ wavelength spectrum.

values, further reducing the bandwidth of the fiber than NT-NCF with $t_2 = 0.65\,\mu m$. It can also be deduced from Fig. 3.3(c) that the 8% elliptic NT-NCF with bi-thickness has higher orthogonal polarization losses and similar resonance points on the higher wavelength values compared to 8% elliptic NT-NCF without bi-thickness.

The PER and birefringence graphs are shown in Fig. 3.3(d) and Fig. 3.3(e), respectively, for NT-NCF and 8% elliptic NT-NCF with and without bi-thickness. In fibers with induced bi-thickness, 8% elliptic NT-NCF shows more PER than NT-NCF, as observed in Fig. 3.3(d). In comparison, 8% elliptic NT-NCFs with bi-thickness and without bi-thickness, the fiber with $t_2 = 0.65\,\mu m$ initially had a lower PER than the fiber with $t_1 = t_2 = 0.41\,\mu m$ but later increased to a higher value at $1.55\,\mu m$ wavelength before achieving minimum. The overall PER values are still very low. The NT-NCF, due to the effect of t_2 showed birefringence in the range 10^{-5}, which was further increased by 8% elliptic NT-NCF as depicted in Fig. 3.3(e). This birefringence was almost more than one order of magnitude higher than the birefringence of 8% elliptic NT-NCF without bi-thickness in the range of $1.4\,\mu m$ to $1.9\,\mu m$ wavelength spectrum.

3.3.3 Manipulation of nested tube diameter (d_{nx}) coupled with ellipticity

In order to get more coupling between horizontal polarization core mode and cladding mode, nested tube diameter d_{nx} was manipulated along the horizontal direction as shown in Fig. 3.4(a). While all the remaining parameters were kept same at $D = 30\,\mu m$, $d = 0.85D$, $d_n = 0.56d$ and $t = 0.41\,\mu m$. In Fig. 3.4(a), when $d_{nx} = d_n$, the NT-NCF was in its original state, as in Fig. 3.1(a), which was incapable of PM operation. Whereas $d_{nx} = 0$ and $d_{nx} = 0.8d$ referred to the absence of the nested tubes and larger nested tube diameter, in the horizontal axis, compared to all the remaining nested tubes, respectively. This resulted in generation of orthogonal polarization modes in NT-NCF as illustrated by confinement loss curves in Fig. 3.4(c). The 8% elliptic NT-NCF structure with altered

d_{nx} is shown in Fig. 3.4(b).

3.3.3.1 Absence of nested tube along fiber horizontal axis ($d_{nx} = 0$)

In NT-NCF, when $d_{nx} = 0$, both polarizations experienced more losses than the original state of NT-NCF ($d_{nx} = d_n$) as depicted in Fig. 3.4(c). This increase in loss was due to the enhanced coupling of horizontal polarization and vertical polarization modes with the cladding modes, which was further increased by 8% elliptic NT-NCF and showed the highest losses for orthogonal polarizations (see Fig. 3.4(c)). Further, the NT-NCF and 8% elliptic NT-NCF fibers with $d_{nx} = 0$ experienced similar PER of around 5 over a broad wavelength range as presented in Fig. 3.4(d). Moreover, Fig. 3.4(e) shows that very little birefringence (in the range of 10^{-7}) was produced by NT-NCF without horizontal nested tubes, while 8% elliptic NT-NCF with $d_{nx} = 0$ had the highest birefringence (in the range of 10^{-6}) which reduced to a minimum point at 1.75 μm wavelength and then started to increase again.

3.3.3.2 Nested tube along fiber horizontal axis with different diameter ($d_{nx} = 0.8d$)

Fig. 3.4(c) illustrates that compared to NT-NCF when $d_{nx} = d_n$, NT-NCF with $d_{nx} = 0.8d$ showed similar losses for vertical polarization, while horizontal polarization loss was slightly higher due to its enhanced coupling with cladding modes. When 8% ellipticity was induced in elliptic NT-NCF with $d_{nx} = 0.8d$, losses for both polarizations increased due to the movement of resonance points from larger to smaller wavelengths. It is worth noting that horizontal polarization showed more coupling with the cladding modes, due to which there is a greater loss separation between vertical polarization and horizontal polarization in 8% elliptic NT-NCF with $d_{nx} = 0.8d$ (refer to Fig. 3.4(c)). This observation was well supported by PER values of more than 10 in between 1 μm to 1.6 μm wavelength spectrum reaching the highest PER of 24 at 1.5 μm wavelength for 8% elliptic NT-NCF with $d_{nx} = 0.8d$ as presented in Fig. 3.4(d). Fig. 3.4(e) depicts that

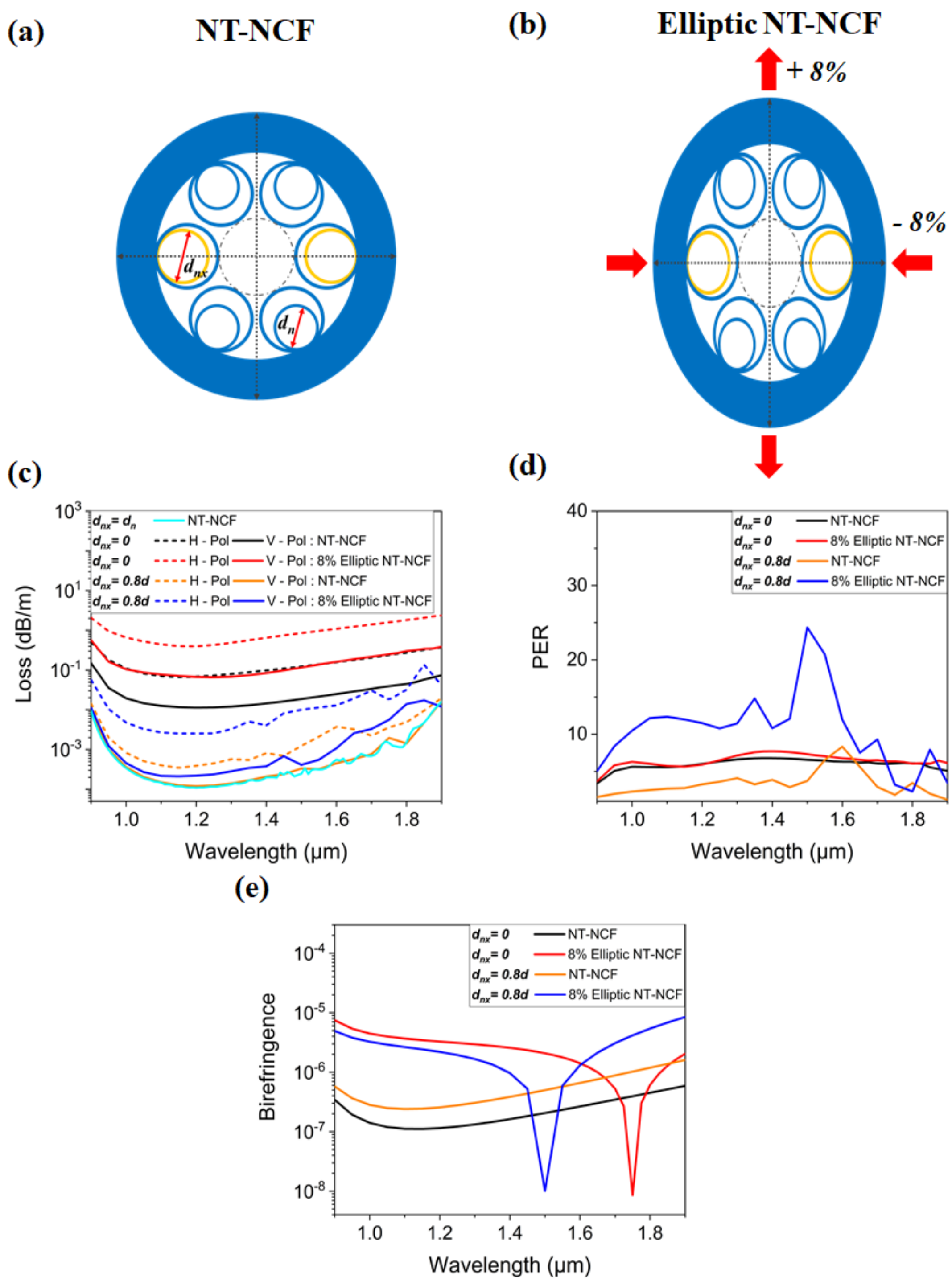

Figure 3.4: Schematic illustration of the implementation of different nested tube diameter d_{nx} along the horizontal direction in (a) NT-NCF design and (b) 8% elliptic NT-NCF design, (c) confinement loss comparison, (d) PER comparison, and (e) birefringence comparison between NT-NCF and 8% elliptic NT-NCF designs with $d_{nx} = d_n$, $d_{nx} = 0$, and $d_{nx} = 0.8d$ from 0.9 μm to 1.9 μm wavelength spectrum.

the birefringence with $d_{nx} = 0.8d$ for NT-NCF was lower (in the range of 10^{-7}) compared to the higher birefringence of 8% elliptic NT-NCF which was on the order of 10^{-6}.

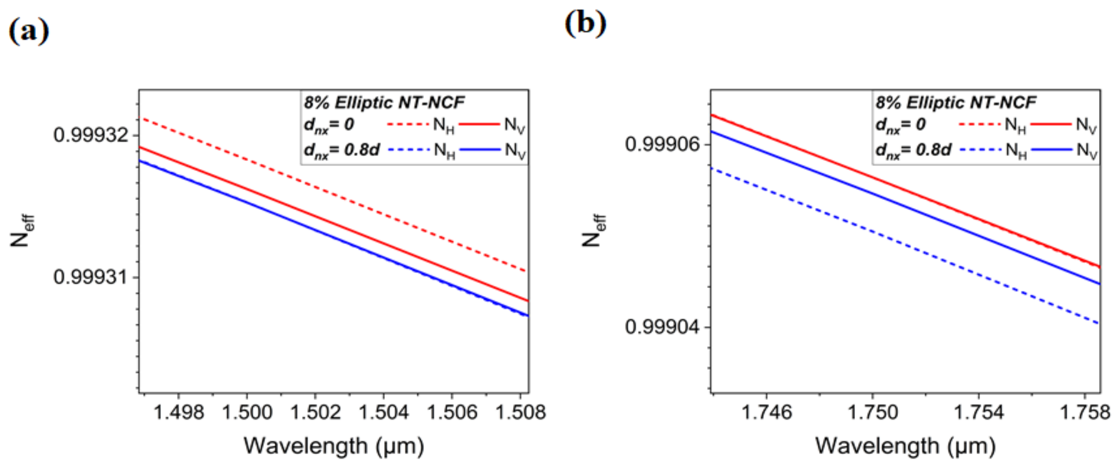

Figure 3.5: Effective refractive index (N_{eff}) graph of horizontal polarization (N_H) and vertical polarization (N_V) effective indices against wavelength spectrum for 8% Elliptic NT-NCF structure with $d_{nx} = 0$ and $d_{nx} = 0.8d$. The crossing points of N_H and N_V curves (a) at 1.5 μm wavelength for $d_{nx} = 0.8d$ and (b) at 1.75 μm wavelength for $d_{nx} = 0$.

The alteration of d_{nx} coupled with ellipticity led to the lowest losses with the highest PER for 8% elliptic NT-NCF with $d_{nx} = 0.8d$ (see Fig. 3.4(c) and Fig. 3.4(d)). This fiber configuration favored more horizontal polarization mode coupling with cladding modes therefore high PER was achieved. However, the achieved PER of 24 is still lower than the recommended PER of > 100 [47] for satisfactory PM operation.

Although the birefringence achieved was on the order of 10^{-6} by 8% elliptic NT-NCF with both $d_{nx} = 0$ and $d_{nx} = 0.8d$, the fiber with no nested tubes along horizontal direction showed slightly higher birefringence values (refer to Fig. 3.4(e)). The high birefringence produced by elliptic fiber with $d_{nx} = 0$ compared to the elliptic fiber with $d_{nx} = 0.8d$ is because the minimum birefringence for elliptic fiber with $d_{nx} = 0.8d$ was reached before than the minimum birefringence of elliptic fiber with $d_{nx} = 0$ as observed in Fig. 3.4(e). This means that the N_H and N_V curves crossed each other at a smaller wavelength for fiber with

$d_{nx} = 0.8d$ as shown in Fig. 3.5(a), resulting in a smaller difference between N_H and N_V at adjacent wavelengths, thus reducing birefringence. In contrast, for the fiber with no nested tube along the horizontal axis, N_H and N_V curves crossed each other at a larger wavelength as illustrated in Fig. 3.5(b), which led to higher birefringence. The overall birefringence of the fibers is very low compared to commercial PM fibers' birefringence level of more than 10^{-4}.

Chapter 4

Conclusion

In conclusion, the first part of the thesis presented the design and optimization of a novel polarization-maintaining and spectral filtering negative curvature hollow-core fiber (NCF). The proposed P-PMNCF structure, with its unique nested tube arrangement and pole structure, demonstrates excellent performance in terms of polarization preservation and selective transmission. By systematically varying the cladding tube thickness, t_2, nested tube diameter, d_2, pole length, L_p, and ellipticity, D_x, we achieved improvement in confinement losses and birefringence levels. The parameters t_2 and D_x contributed to the enhancement of birefringence when t_2 is increased in the vicinity of the resonance region and D_x is decreased, respectively. In contrast, the remaining parameters d_2 and L_p, when increased, exhibited a minor negative effect on birefringence. However, the filtered wavelength losses in the vertically polarized state were still maintained below the target. The optimized fiber design showed a transmission loss below 0.1 dB/km for filtered wavelengths and a birefringence on the order of 10^{-5}. Compared to our previous study [64], this proposed fiber design exhibited improved performance with reduced losses, better polarization extinction ratio, high birefringence, and a narrower range of filtered wavelengths. These findings demonstrate the potential of the proposed P-PMNCF for applications requiring simultaneous polarization maintenance and spectral filtering. Furthermore, the P-PMNCF fiber is capable of sensing chemicals and gases as long as its birefringence aligns with the application requirements. However, external factors like pressure or temperature could affect the performance of the fiber if they lead to major changes that are greater than the birefringence of fiber. Future work can explore additional design optimization and investigate the practical implementation of fiber design in various optical systems and devices.

In the second part of the thesis, we explored the effects of ellipticity on polarization maintaining (PM) operation of nested tube negative curvature hollow-core fiber (NT-NCF). We started with an optimized design of a six-tube NT-NCF with an isotropic core, which was incapable of generating orthogonal polarization modes. Subsequently, the NT-NCF was subjected to elongation and contraction in vertical and horizontal axes with 5%, 8%, and 10% ellipticity. These alterations made the entire fiber elliptic, which we termed as Elliptic NT-NCF, causing the fiber core, all cladding elements, and the outer fiber ring to become elliptic. The introduction of ellipticity broke the fiber core symmetry, enabling Elliptic NT-NCF to support PM operation. We further investigated the impact of 8% Elliptic NT-NCF coupled with bi-thickness (t_1 and t_2) and altered nested tube diameter (d_{nx}) on PM properties of the fiber. Our findings indicate that ellipticity has minor effects on enhancing birefringence and polarization extinction ratio (PER) in PM-NCFs. Nevertheless, ellipticity can aid in fine-tuning the PM properties. Moreover, we also learned that the introduction of t_2 in the fiber shifted the resonance points residing on lower wavelength points to the higher wavelength points, whereas ellipticity moved the resonance points on larger wavelengths to smaller wavelengths. Therefore, similar to the effect of thickness, ellipticity reduces the bandwidth of fiber. The highest birefringence and PER achieved with 8% Elliptic NT-NCF was on the order of 10^{-5} and 24, respectively. Although ellipticity has a limited impact on obtaining high birefringence and PER, it provides a useful supplementary tuning mechanism in PM-NCFs.

Bibliography

[1] K. C. Kao and G. A. Hockham, “Dielectric-fibre surface waveguides for optical frequencies,” in *Proceedings of the Institution of Electrical Engineers*, vol. 113, pp. 1151–1158, IET, 1966.

[2] R. J. Mears, L. Reekie, I. Jauncey, and D. N. Payne, “Low-noise erbium-doped fibre amplifier operating at 1.54 μm,” *Electronics Letters*, vol. 19, no. 23, pp. 1026–1028, 1987.

[3] D. P. Hand, J. D. Entwistle, R. R. Maier, A. Kuhn, C. A. Greated, and J. D. Jones, “Fibre optic beam delivery system for high peak power laser piv illumination,” *Measurement Science and Technology*, vol. 10, no. 3, p. 239, 1999.

[4] Y. e. Jeong, J. Sahu, D. Payne, and J. Nilsson, “Ytterbium-doped large-core fiber laser with 1.36 kw continuous-wave output power,” *Optics express*, vol. 12, no. 25, pp. 6088–6092, 2004.

[5] E. Maurice, G. Monnom, B. Dussardier, A. Saïssy, D. B. Ostrowsky, and G. W. Baxter, “Erbium-doped silica fibers for intrinsic fiber-optic temperature sensors,” *Appl. Opt.*, vol. 34, pp. 8019–8025, Dec 1995.

[6] G.-D. Peng, *Handbook of Optical Fibers.* Springer, 2019.

[7] P. S. J. Russell, “Photonic-crystal fibers,” *Journal of lightwave technology*, vol. 24, no. 12, pp. 4729–4749, 2006.

[8] P. S. J. Russell, P. Hölzer, W. Chang, A. Abdolvand, and J. Travers, "Hollow-core photonic crystal fibres for gas-based nonlinear optics," *Nature Photonics*, vol. 8, no. 4, pp. 278–286, 2014.

[9] B. Debord, F. Amrani, L. Vincetti, F. Gérôme, and F. Benabid, "Hollow-core fiber technology: The rising of "gas photonics"," *Fibers*, vol. 7, no. 2, p. 16, 2019.

[10] C. Wei, R. J. Weiblen, C. R. Menyuk, and J. Hu, "Negative curvature fibers," *Advances in Optics and Photonics*, vol. 9, no. 3, pp. 504–561, 2017.

[11] F. Poletti, M. N. Petrovich, and D. J. Richardson, "Hollow-core photonic bandgap fibers: technology and applications," *Nanophotonics*, vol. 2, no. 5-6, pp. 315–340, 2013.

[12] P. Roberts, F. Couny, H. Sabert, B. Mangan, D. Williams, L. Farr, M. Mason, A. Tomlinson, T. A. Birks, J. C. Knight, *et al.*, "Ultimate low loss of hollow-core photonic crystal fibres," *Optics express*, vol. 13, no. 1, pp. 236–244, 2005.

[13] R. Cregan, B. Mangan, J. C. Knight, T. A. Birks, P. S. J. Russell, P. Roberts, and D. Allan, "Single-mode photonic band gap guidance of light in air," *science*, vol. 285, no. 5433, pp. 1537–1539, 1999.

[14] F. e. Poletti, N. Wheeler, M. Petrovich, N. Baddela, E. Numkam Fokoua, J. Hayes, D. Gray, Z. Li, R. Slavík, and D. Richardson, "Towards high-capacity fibre-optic communications at the speed of light in vacuum," *Nature Photonics*, vol. 7, no. 4, pp. 279–284, 2013.

[15] F. Benabid and P. Roberts, "Guidance mechanisms in hollow-core photonic crystal fiber," in *Photonic Crystal Materials and Devices VII*, vol. 6901, pp. 176–185, SPIE, 2008.

[16] Y. Wang, M. Alharbi, T. D. Bradley, C. Fourcade-Dutin, B. Debord, B. Beaudou, F. Gerôme, and F. Benabid, "Hollow-core photonic crystal fibre for high power laser beam delivery," *High Power Laser Science and Engineering*, vol. 1, no. 1, pp. 17–28, 2013.

[17] N. Litchinitser, A. Abeeluck, C. Headley, and B. Eggleton, "Antiresonant reflecting photonic crystal optical waveguides," *Optics letters*, vol. 27, no. 18, pp. 1592–1594, 2002.

[18] A. W. Snyder, J. D. Love, *et al.*, *Optical waveguide theory*, vol. 175. Chapman and hall London, 1983.

[19] G. Renversez, P. Boyer, and A. Sagrini, "Antiresonant reflecting optical waveguide microstructured fibers revisited: a new analysis based on leaky mode coupling," *Optics Express*, vol. 14, no. 12, pp. 5682–5687, 2006.

[20] F. Benabid, J. C. Knight, G. Antonopoulos, and P. S. J. Russell, "Stimulated raman scattering in hydrogen-filled hollow-core photonic crystal fiber," *Science*, vol. 298, no. 5592, pp. 399–402, 2002.

[21] G. Pearce, G. Wiederhecker, C. G. Poulton, S. Burger, and P. S. J. Russell, "Models for guidance in kagome-structured hollow-core photonic crystal fibres," *Optics express*, vol. 15, no. 20, pp. 12680–12685, 2007.

[22] Y. Wang, F. Couny, P. Roberts, and F. Benabid, "Low loss broadband transmission in optimized core-shape kagome hollow-core pcf," in *Conference on Lasers and Electro-Optics*, p. CPDB4, Optica Publishing Group, 2010.

[23] A. N. Kolyadin, A. F. Kosolapov, A. D. Pryamikov, A. S. Biriukov, V. G. Plotnichenko, and E. M. Dianov, "Light transmission in negative curvature hollow core fiber in extremely high material loss region," *Optics express*, vol. 21, no. 8, pp. 9514–9519, 2013.

[24] M. Michieletto, J. K. Lyngsø, C. Jakobsen, J. Lægsgaard, O. Bang, and T. T. Alkeskjold, "Hollow-core fibers for high power pulse delivery," *Optics express*, vol. 24, no. 7, pp. 7103–7119, 2016.

[25] F. Poletti, "Nested antiresonant nodeless hollow core fiber," *Optics express*, vol. 22, no. 20, pp. 23807–23828, 2014.

[26] Y. Wang, N. V. Wheeler, F. Couny, P. Roberts, and F. Benabid, "Low loss broadband transmission in hypocycloid-core kagome hollow-core photonic crystal fiber," *Optics letters*, vol. 36, no. 5, pp. 669–671, 2011.

[27] F. Yu and J. Knight, "Negative curvature hollow core optical fiber," *IEEE Journal of Selected Topics in Quantum Electronics*, vol. 22, no. 2, pp. 1–11, 2016.

[28] F. Yu, W. J. Wadsworth, and J. C. Knight, "Low loss silica hollow core fibers for 3–4 μm spectral region," *Optics express*, vol. 20, no. 10, pp. 11153–11158, 2012.

[29] T. D. Bradley, J. R. Hayes, Y. Chen, G. T. Jasion, S. R. Sandoghchi, R. Slavík, E. N. Fokoua, S. Bawn, H. Sakr, I. A. Davidson, *et al.*, "Record low-loss 1.3 db/km data transmitting antiresonant hollow core fibre," in *2018 European Conference on Optical Communication (ECOC)*, pp. 1–3, IEEE, 2018.

[30] G. T. Jasion, H. Sakr, J. R. Hayes, S. R. Sandoghchi, L. Hooper, E. N. Fokoua, A. Saljoghei, H. C. Mulvad, M. Alonso, A. Taranta, *et al.*, "0.174 db/km hollow core double nested antiresonant nodeless fiber (dnanf)," in *2022 Optical Fiber Communications Conference and Exhibition (OFC)*, pp. 1–3, IEEE, 2022.

[31] Y. Chen, M. Petrovich, E. N. Fokoua, A. Adamu, M. Hassan, H. Sakr, R. Slavík, S. B. Gorajoobi, M. Alonso, R. F. Ando, *et al.*, "Hollow core dnanf optical fiber with¡ 0.11 db/km loss," in *Optical Fiber Communication Conference*, pp. Th4A–8, Optica Publishing Group, 2024.

[32] C. Emslie, "Polarization maintaining fibers," *Specialty Optical Fibers Handbook*, p. 243, 2011.

[33] M. A. Terrel, M. J. Digonnet, and S. Fan, "Resonant fiber optic gyroscope using an air-core fiber," *Journal of lightwave technology*, vol. 30, no. 7, pp. 931–937, 2011.

[34] A. Rahman, A. Khaleque, M. Y. Ali, and M. T. Rahman, "Thz spectroscopic sensing of liquid chemicals using a photonic crystal fiber," *OSA Continuum*, vol. 3, no. 11, pp. 2982–2996, 2020.

[35] A. D. Slepkov, A. R. Bhagwat, V. Venkataraman, P. Londero, and A. L. Gaeta, "Spectroscopy of rb atoms in hollow-core fibers," *Physical Review A—Atomic, Molecular, and Optical Physics*, vol. 81, no. 5, p. 053825, 2010.

[36] X. Peng and L. Dong, "Fundamental-mode operation in polarization-maintaining ytterbium-doped fiber with an effective area of 1400 μm 2," *Optics letters*, vol. 32, no. 4, pp. 358–360, 2007.

[37] T. Hosaka, K. Okamoto, T. Miya, Y. Sasaki, and T. Edahiro, "Low-loss single polarisation fibres with asymmetrical strain birefringence," *Electronics Letters*, vol. 15, no. 17, pp. 530–531, 1981.

[38] R. Birch, D. N. Payne, and M. Varnham, "Fabrication of polarisation-maintaining fibres using gas-phase etching," *Electronics Letters*, vol. 24, no. 18, pp. 1036–1038, 1982.

[39] R. B. Dyott, J. Cozens, and D. Morris, "Preservation of polarisation in optical-fibre waveguides with elliptical cores," *Electronics Letters*, vol. 15, no. 13, pp. 380–382, 1979.

[40] S. A. Mousavi, S. R. Sandoghchi, D. J. Richardson, and F. Poletti, "Broadband high birefringence and polarizing hollow core antiresonant fibers," *Optics express*, vol. 24, no. 20, pp. 22943–22958, 2016.

[41] W. Belardi and J. C. Knight, "Hollow antiresonant fibers with low bending loss," *Optics express*, vol. 22, no. 8, pp. 10091–10096, 2014.

[42] F. Couny, F. Benabid, P. Roberts, P. Light, and M. Raymer, "Generation and photonic guidance of multi-octave optical-frequency combs," *Science*, vol. 318, no. 5853, pp. 1118–1121, 2007.

[43] F. Emaury, C. J. Saraceno, B. Debord, D. Ghosh, A. Diebold, F. Gèrôme, T. Südmeyer, F. Benabid, and U. Keller, "Efficient spectral broadening in the 100-w average power regime using gas-filled kagome hc-pcf and pulse compression," *Optics Letters*, vol. 39, no. 24, pp. 6843–6846, 2014.

[44] P. S. J. Russell, P. Hölzer, W. Chang, A. Abdolvand, and J. Travers, "Hollow-core photonic crystal fibres for gas-based nonlinear optics," *Nature Photonics*, vol. 8, no. 4, pp. 278–286, 2014.

[45] F. Benabid and P. Roberts, "Linear and nonlinear optical properties of hollow core photonic crystal fiber," *Journal of Modern Optics*, vol. 58, no. 2, pp. 87–124, 2011.

[46] W. Ding and Y.-Y. Wang, "Hybrid transmission bands and large birefringence in hollow-core anti-resonant fibers," *Optics Express*, vol. 23, no. 16, pp. 21165–21174, 2015.

[47] M. S. Hosen, A. Khaleque, K. S. R. Shaha, L. N. Asha, A. S. Sultana, R. Nishad, and M. T. Rahman, "Highly birefringent polarization maintaining low-loss single-mode hollow-core antiresonant fiber," *Optics Continuum*, vol. 1, no. 10, pp. 2167–2184, 2022.

[48] S. Wei, Y. Zhang, T. Wu, Z. Hou, C. Xia, J. Liu, and G. Zhou, "Broadband birefringence hollow-core anti-resonant optical fiber with elliptical air holes," *Optics Communications*, vol. 527, p. 128976, 2023.

[49] Y. Hong, A. Jia, S. Gao, Y. Sheng, X. Lu, Z. Liang, Z. Zhang, W. Ding, and Y. Wang, "Birefringent, low loss, and broadband semi-tube anti-resonant hollow-core fiber," *Optics Letters*, vol. 48, no. 1, pp. 163–166, 2023.

[50] A. D. Slepkov, A. R. Bhagwat, V. Venkataraman, P. Londero, and A. L. Gaeta, "Spectroscopy of rb atoms in hollow-core fibers," *Physical Review A—Atomic, Molecular, and Optical Physics*, vol. 81, no. 5, p. 053825, 2010.

[51] X. Peng and L. Dong, "Fundamental-mode operation in polarization-maintaining ytterbium-doped fiber with an effective area of 1400 μm 2," *Optics letters*, vol. 32, no. 4, pp. 358–360, 2007.

[52] R. Yu, Y. Chen, L. Shui, and L. Xiao, "Hollow-core photonic crystal fiber gas sensing," *Sensors*, vol. 20, no. 10, p. 2996, 2020.

[53] X. Huang, J. Zang, and S. Yoo, "Sensing applications of double hollow-core anti-resonant fiber based modal interferometer," in *CLEO: Applications and Technology*, pp. AF1M–3, Optica Publishing Group, 2018.

[54] H. Jia, X. Wang, T. M. Benson, S. Gu, S. Lou, and X. Sheng, "Ultrawide bandwidth dual sakura hollow-core antiresonant fiber polarization beam splitter," *JOSA B*, vol. 38, no. 11, pp. 3395–3402, 2021.

[55] K. S. R. Shaha, A. Khaleque, M. T. Rahman, and M. S. Hosen, "Broadband and short-length polarization splitter on dual hollow-core antiresonant fiber," *IEEE Photonics Technology Letters*, vol. 34, no. 5, pp. 259–262, 2022.

[56] S. Yerolatsitis, R. Shurvinton, P. Song, Y. Zhang, R. J. Francis-Jones, and K. R. Rusimova, "Birefringent anti-resonant hollow-core fiber," *Journal of Lightwave Technology*, vol. 38, no. 18, pp. 5157–5162, 2020.

[57] Y. Zhu, W. Li, F. Gao, X. Xu, and N. Song, "Small-core hollow-core nested antiresonant nodeless fiber with semi-circular tubes," *Optics Express*, vol. 30, no. 12, pp. 20373–20388, 2022.

[58] S. Choi, T. Eom, J. Yu, B. Lee, and K. Oh, "Novel all-fiber bandpass filter based on hollow optical fiber," *IEEE Photonics Technology Letters*, vol. 14, no. 12, pp. 1701–1703, 2002.

[59] T. Komukai, K. Tamura, and M. Nakazawa, "An efficient 0.04-nm apodized fiber bragg grating and its application to narrow-band spectral filtering," *IEEE Photonics Technology Letters*, vol. 9, no. 7, pp. 934–936, 1997.

[60] N. Dong, S. Wang, L. Jiang, Y. Jiang, P. Wang, and L. Zhang, "Pressure and temperature sensor based on graphene diaphragm and fiber bragg gratings," *IEEE Photonics Technology Letters*, vol. 30, no. 5, pp. 431–434, 2017.

[61] T. Komukai, T. Yamamoto, and S. Kawanishi, "Optical pulse generator using phase modulator and linearly chirped fiber bragg gratings," *IEEE photonics technology letters*, vol. 17, no. 8, pp. 1746–1748, 2005.

[62] Z. Liu, Y. Liu, J. Du, S. Yuan, and X. Dong, "Channel-spacing and wavelength switchable multiwavelength erbium-doped fiber laser using sampled

hi-bi fiber grating and photonic crystal fiber loop mirror," *Laser Physics Letters*, vol. 5, no. 2, p. 122, 2007.

[63] J. Gamble, A. M. Marn, M. Ordu, and A. E. Akosman, "Frequency selective hollow-core negative curvature fiber design via nest-clad poling," in *Specialty Optical Fibers*, pp. SoTu1I–5, Optica Publishing Group, 2022.

[64] J. Gamble, M. Ordu, and A. E. Akosman, "Spectral and polarization filtering in negative curvature hollow core fibers," in *Photonic Fiber and Crystal Devices: Advances in Materials and Innovations in Device Applications XVI*, p. PC1222909, SPIE, 2022.

[65] M. Ordu and A. E. Akosman, "Re-thinking the design of low-loss hollow-core fibers via optimal positioning of the nested elements," *Optics Letters*, vol. 47, no. 12, pp. 3039–3042, 2022.

[66] A. E. Akosman and M. Ordu, "Nested compound negative curvature hollow-core fiber for single-mode operation in the infrared region," *Optics Communications*, vol. 497, p. 127194, 2021.

[67] S. M. Abokhamis Mousavi, *Exploring optical nonlinearity in gas-filled hollow core fibre*. PhD thesis, University of Southampton, 2018.